Mechano-metabolism of metastatic breast cancer cells in 2D and 3D microenvironments.

Anuja Jaganathan[1,2#], Joshua Toth[1,2#], Xingyu Chen[1,2], Ramin Basir [1,2], Laurent Pieuchot[3], Yihui Shen[4], Cynthia Reinhart-King[5], Vivek B. Shenoy[1,2,4,6*]

[1]Center for Engineering Mechanobiology, University of Pennsylvania, PA, US
[2]Department of Materials Science and Engineering, University of Pennsylvania, PA, US
[3]Université de Haute-Alsace, CNRS, IS2M UMR 7361, Mulhouse 68100, France
[4]Department of Bioengineering, University of Pennsylvania, PA, US
[5]Department of Biomedical Engineering, Vanderbilt University, Nashville, TN 37235, US
[6]Department of Mechanical Engineering and Applied Mathematics, University of Pennsylvania, PA, US

[#]Equal Contribution

*Correspondence to Vivek B. Shenoy vshenoy@seas.upenn.edu
Email: vshenoy@seas.upenn.edu

Abstract

Cells regulate their shape and metabolic activity in response to the mechano-chemical properties of their microenvironment. To elucidate the impact of matrix stiffness and ligand density on the bioenergetics of mesenchymal cells, we developed a nonequilibrium, active chemo-mechanical model that accounts for the mechanical energy of the cell and matrix, chemical energy from ATP hydrolysis, interfacial energy, and mechano-sensitive regulation of stress fiber assembly through signaling. By integrating the kinetics and energetics of these processes, we define the cell "metabolic potential" that, when minimized, provides testable predictions of cell contractility, shape, and ATP consumption. Specifically, we show that the morphology of MDA-MB-231 breast cancer cells in 3D collagen changes from spherical to elongated to spherical with increasing matrix stiffness, which is consistent with experimental observations. On 2D hydrogels, our model predicts a hemispherical-to-spindle-to-disc shape transition with increasing gel stiffness. In both cases, we show that these shape transitions emerge from competition between the energy of ATP hydrolysis associated with increased contractility that drives cell elongation and the interfacial energy that favors a rounded shape. Furthermore, our model can predict how increased energy demand in stiffer microenvironments is met by AMPK activation, which is confirmed experimentally in both 2D and 3D microenvironments and found to correlate with the upregulation of mitochondrial potential, glucose uptake, and ATP levels, as well as provide estimates of changes in intracellular adenosine nucleotide concentrations with changing environmental stiffness. Overall, we present a framework for relating adherent cell energy levels and contractility through biochemical regulation of underlying physical processes.

Statement of Significance

Increasing evidence indicates that cellular metabolism is regulated by mechanical cues from the extracellular environment. Forces transmitted from the microenvironment activate mechanotransduction pathways in the cell, which trigger a cascade of biochemical events that impact cytoskeletal tension, cellular morphology and energy budget available to the cell. Using a nonequilibrium free energy-based theory, we can predict the ATP consumption, contractility, and shape of mesenchymal cancer cells, as well as how cells regulate energy levels dependent on the mechanosensitive metabolic regulator AMPK. The insights from our model can be used to understand the mechanosensitive regulation of metabolism during metastasis and tumor progression, during which cells experience dynamic changes in their microenvironment and metabolic state.

Introduction

Cells feel and respond to their mechanical environment through reorganization of the cytoskeletal architecture and control of actomyosin contractility[1]. Many studies link changes in contractility to changes in cell stiffness[2], cell shape[3], and cell differentiation[4,5] as the result of mechanosensitive biochemical pathways. It has also been shown that the mechanical environment of cells can regulate metabolic changes via a myriad of different mechanisms influencing, for example, cytoskeletal sequestration of glycolytic enzymes[6–9], lipid synthesis[10,11], mitochondrial shape and function[12,13], and YAP/TAZ signaling[14,15]. However, the most immediate outcome impacting cellular energy availability in the context of a changing mechanical environment is the upregulation of adenosine triphosphate (ATP) production in response to increasing environmental stiffness through activation of the master metabolic regulator 5' adenosine monophosphate-activated protein kinase (AMPK)[16–18]. As a sensor of intracellular energy levels, the regulation of the activity of this kinase affects several downstream pathways responsible for controlling the extent to which metabolic processes such as glucose uptake[19,20], glycolysis[21,22], oxidative phosphorylation (OXPHOS)[23], protein synthesis[24], and autophagy[25] occur. Thus, there is a clear connection between the energy-intensive processes involved in the generation and maintenance of cell contractility and the need for AMPK to regulate the availability of energy within contractile cells. Mechanotransduction and its role in regulating metabolism have physiological relevance, particularly in determining cancer cell migration, tumor progression and metastasis[26,27], with cancer cells reprogramming their metabolism in response to mechanical

cues from the local microenvironment[28]. Studies investigating this interplay between forces transmitted from the ECM and cell metabolism in response to the mechanical microenvironment have been largely qualitative in nature. Therefore, predictive mathematical models that provide a unified framework to model the kinetics of mechano-signaling and the mechano-sensitive modulation of the energy available to cells can offer quantitative insight into the mechanisms governing the mechanosensitive nature of cell energetics and metabolism.

Here, we develop a chemo-mechanical model for contractility and adhesion based on the concept of a "metabolic potential" by explicitly accounting for the conversion of energy from ATP hydrolysis linked to myosin-II motor activity to both conservative chemical and mechanical energies associated with cell contractility and dissipative heat. We show that since these energies are modulated by mechanosensitive signaling pathways regulating stress fiber assembly kinetics, the contractility and morphology of cells are altered to *minimize their metabolic potential* in different microenvironments. We utilize this metabolic potential to make predictions regarding optimum cell shapes, contractility, and ATP consumption in environments with changing stiffness. Furthermore, we predict that distinct differences in optimum cell shapes between cells on 2D substrates and cells in 3D matrices arise purely because of variations in the distribution of stresses generated as a consequence of differences in the geometry that impact downstream chemo-mechanical signaling. Additionally, we introduce a theoretical framework for the replenishment of intracellular energy stores in response to the upregulation of energy-consuming processes such as stress fiber assembly by considering the parallel activation of AMPK. We show how, counterintuitively, intracellular ATP can be maintained at higher levels in highly contractile cells as a result of this homeostatic pathway. Our model makes testable predictions regarding cell morphology, contractility, and metabolic activity, which we validate with experiments measuring cell shapes and intracellular ATP:ADP ratios of MDA MB-231 cells in environments of different stiffnesses. MDA MB-231 are triple negative breast cancer cells which is the most aggressive breast cancer phenotype with a high metastatic potential[29], hence forming an ideal choice for this study. We also find that levels of cell glucose uptake and the mitochondrial membrane potential correlate well with the predicted AMPK activity. Our model thus provides a predictive quantitative tool for studying the interplay between mechanosensitive changes in cellular morphology, contractility, signaling and metabolism.

Results

Mathematical formulation of a metabolic potential for adherent cells

In adherent contractile mesenchymal cells, myosin-II motors bind to F-actin filaments and generate contractile forces though the assembly of stress fibers in the process converting energy released through ATP hydrolysis into mechanical work[30,31]. Cell contraction generates tensile stresses in the cytoskeleton, particularly in stiffer microenvironments, which in turn can trigger mechanosensitive pathways such as the Rho-ROCK[32,33] and the Ca^{2+}/calmodulin pathways[34] (Figure 1a), which has the overall effect of increasing the rate of stress fiber assembly (Figure S1). Consequently, the dynamic steady-state is shifted to more stable stress fibers, and the cells adopt a higher steady-state level of contractility (or a higher density of engaged or "active" motors) in response to stiff microenvironments. Thus, stress-regulated mechano-signaling directly leads to increased ATP consumption (in a time-averaged sense) on stiffer substrates. We first formulate the metabolic potential for a cell held between two microposts[35] (Figure S3a) with the goal of predicting how the cytoskeletal contractility is modulated by the stiffness of the extracellular microenvironment and how the change in contractility is directly correlated with the amount of ATP consumed. This analysis lays the groundwork for the more general case of cells in 3D collagen networks and 2D gels.

<u>*A 1D model for cells adhered to microposts*</u> To understand the key principles that underpin the concept of mechanosensitive metabolism in our model, we first consider the simple 1D case of a cell adhered to microposts (Figure S3a). The cell is represented by elastic (representing the passive mechanical components of the cytoskeleton) and active contractile (representing stress fibers) components, while the microposts are modeled as elastic elements in series with the cell (Figure S3a). We treat molecular myosin motors as force dipoles (Figure S2), and the contractile stress, or contractility, generated by the motors engaged in the stress fibers is represented by the variable ρ (Figure S2), while the cytoskeletal stress and strain generated in the cell are denoted as σ and ϵ, respectively. In the quiescent (non-adhered) cell, we assume that the cell displays a baseline level of contractility, ρ_0, determined by a balance between the decrease in enthalpic interactions when motors bind to actin and the associated loss in entropy compared to that of free motors in the cytosol. As a cell adhered to microposts evolves toward a dynamic steady state, part of the energy available from the hydrolysis of ATP is converted into other forms of energy associated with the assembly of new stress fibers (Figure 1b), namely, i) the chemical energy required for myosin to bind to actin ($U_{binding}(\rho,\epsilon)$), ii) the work done by myosin motors ($U_{motor}(\rho,\epsilon)$ and iii) the strain energy of the cytoskeleton ($U_{strain}^{cell}(\rho,\epsilon)$) and the matrix ($U_{strain}^{ECM}$) (refer to SI Section 1 for detailed derivation).

To formulate an expression for the energy available from ATP hydrolysis, we consider the mechanosensitive nature of myosin motor activity and introduce the kinetic constants $k_{on}(\sigma)$ and $k_{off}(\sigma)$, which represent the stress-sensitive rates of stress fiber assembly and disassembly, respectively Physically, these rate parameters are related to the time required for stress fiber assembly and the lifetime of stress fibers (Figure S1). In particular, a low rate of stress fiber disassembly implies that the stress fibers remain intact and exert contractile forces for longer periods, i.e., $k_{off} \propto \left(1/\tau_{off}\right)$, where τ_{off} is the lifetime of the stress fibers (Figure S1). Hence, the fraction of the time over which a myosin motor is engaged with actin stress fibers and hydrolyzes ATP can be written in terms of the rates as $\tilde{\tau} = \frac{k_{on}(\sigma)}{k_{on}(\sigma)+k_{off}(\sigma)}$; when the rate of stress fiber assembly is high and the disassembly rate is low, the normalized myosin motor engagement time and ATP consumption are maximized. Then, the *time-averaged* energy released by ATP hydrolysis due to myosin activity when the cell reaches a steady state can be written (SI Section 1.1.3) as $U_{ATP} = \tilde{\tau}\rho\Delta\tilde{G}$, where $\tilde{\tau}\rho$ represents the time-averaged density of stress fibers that hydrolyze ATP and do

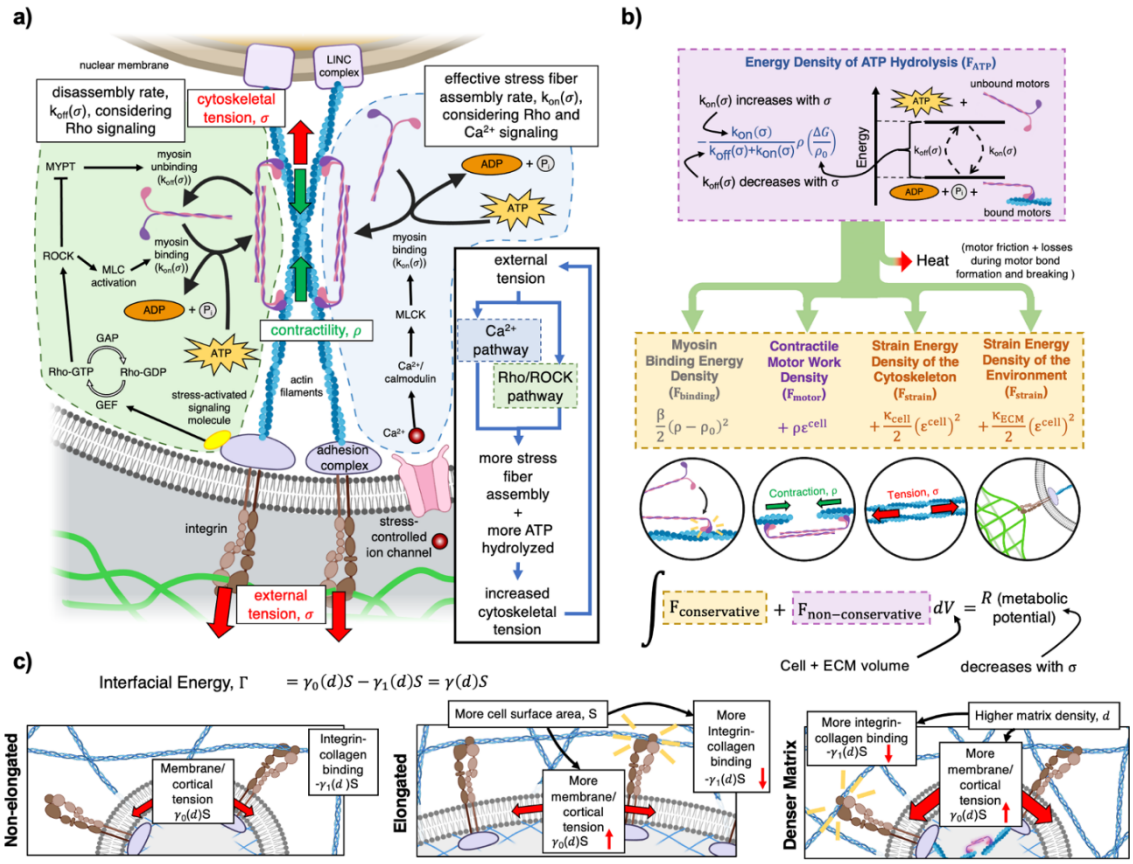

Figure 1: A model for the establishment of stress-regulated contractility driven by ATP hydrolysis. (a) Schematic illustrating the stress-dependent pathways (Rho-ROCK and Ca^{2+} pathways) that regulate cell contractility. Tensile forces transmitted from the micro-environment act on adhesion complexes at the cell-matrix interface and trigger the following bio-chemical processes: (I) The stress-assisted activation of signaling molecules (like Src Family Kinases (SFKs)), which act on Rho-GTPases and enhance Rho activity, promoting ROCK-mediated phosphorylation of myosin light chain (MLC) and consequently, motor recruitment. ROCK activation also leads to inhibition of myosin phosphatase (MYPT) which downregulates myosin unbinding. (II) The generation of cell membrane tension leading to the opening of stress-controlled ion-channels resulting in an influx of Ca^{2+} into the cytoplasm and upregulation of motor activation by myosin light chain kinase (MLCK) activation. Both processes lead to a net increase in the density of stress fibers and more ATP hydrolysis. (b) Schematic showing the breakdown of energies considered in the metabolic potential for the cell. The energy released by ATP hydrolysis (F_{ATP}) depends on the kinetics of stress fiber assembly and comprises the dissipative part of the energy, some of which is converted into conservative forms such as the motor work (F_{motor}), the chemical energy required to bind myosin motors to actin filaments ($F_{binding}$), and the strain energy of the cytoskeleton and ECM (F_{strain}), while the rest is dissipated as heat. (c) The interfacial energy is comprised of two contributions: the membrane/cortical tension, γ_0, which resists any increase in the cell surface area and the adhesion energy of integrin-collagen binding, γ_1, which favors cell elongation as more integrin-ligand bonds can form on the increased surface area of an elongated cell.

mechanical work, while $\Delta\tilde{G} = \Delta G/p_0$ is the amount of energy released by a single myosin motor (ΔG is the energy released from the hydrolysis of an ATP molecule and p_0 is the dipole strength of a single myosin dipole).

A metabolic potential for cells adherent to microposts The energy available from ATP hydrolysis drives otherwise energetically unfavorable processes such as increases in cellular contractility, cytoskeletal remodeling and cell polarization. Hence, we introduce here a cell "metabolic potential", which denotes its ability to hydrolyze ATP and drive energetically unfavorable processes, accounting for the effect of mechano-signaling through the stress-regulated kinetics of stress fiber assembly and disassembly. We define the metabolic potential R as the sum of the conservative energies and the energy of ATP hydrolysis and show (see SI Section 1.1.4) that *minimizing the metabolic potential of the cell with respect to contractility and strain is equivalent to predicting dynamic steady state on the basis of the kinetics of stress fiber formation and disassembly consistent with the Second Law of Thermodynamics.* For cells adherent to microposts, we show (refer to SI Section 1) that the minimum metabolic potential predicts an increasing level of steady-state contractility with increasing micropost stiffness (Figure S3b). Furthermore, the steady-state cell force predicted by the model increases with post stiffness and shows good agreement with the experimentally measured steady-state force exerted by myoblasts contracting against a deformable plate[35,36]. The higher contractility and force on stiff posts is because the elevated rates of mechano-signaling now ensure that ATP hydrolysis is a downhill process, that when coupled with an unfavorable process (such as increased myosin motor contraction, which leads to higher binding and strain energies), makes it energetically feasible. The coupling is regulated by stress such that the rate of stress fiber assembly (k_{on}) is increased, while the fiber disassembly rates (k_{off}) are decreased

(see SI Section 1.1.3). However, the kinetics of mechanosensitive stress fiber formation can depend on the cell type and the myosin II isoform in question. It has been reported that the rate of motor disengagement decreases under tension for myosin IIB due to its strong catch-bond properties[37], consequently leading to longer fiber lifetimes (lower k_{off}). Additionally, an increase in myosin IIB recruitment (and consequently k_{on}) in response to force) is much less prominent and cell type specific[38] and depends on the copolymerization of IIB with IIA[39]. On the other hand, myosin IIA is strongly recruited by actin filaments (the on-rate k_{on} increases) under tension[37], but its catch bond behavior is much weaker than that of IIB[39]. Hence, if we assume the on-rate to be an increasing function of stress and the off-rate to be a decreasing function of stress, the enhanced sensitivity of myosin IIA recruitment to stress and the strong catch-bond property of myosin IIB are captured. Thus, this functional dependence on stress assigned to the two rates (Eq. S1.22) accounts for both the effects of mechano-signaling affecting motor activation and the effects of different myosin isoforms on the kinetics of stress fiber formation and disassembly.

A 3D chemo-mechanical formulation of the metabolic potential
The generalized 3D expression for the conservative energies and the energy of ATP hydrolysis can be formulated in a similar manner (Eq. 2 in Materials and Methods). However, within the 3D framework, the contractility, stress and strain fields are treated as tensor quantities, denoted as ρ_{ij}, σ_{ij} and ϵ_{ij}, , respectively. In elongated cells, stress concentration near the elongated edges (Figure S4a) triggers mechano-signaling pathways leading to preferential formation of stress fibers along the elongated axes and polarized contractility field (i.e., $\rho_{11} \neq \rho_{22} \neq \rho_{33}$). To represent this polarization, rate parameters governing stress fiber assembly $k_{on,ij}$ and disassembly $k_{off,ij}$ are considered to be anisotropic tensor quantities themselves, the volumetric parts of which ($k_{on}^{v}(\sigma_{kk}(\mathbf{x}))$ and $k_{off}^{v}(\sigma_{kk}(\mathbf{x}))$) capture overall changes in assembly rates dependent on mean stress, and the deviatoric parts ($\tilde{k}_{on,ij}(\tilde{\sigma}_{ij}(\mathbf{x}))$ and $\tilde{k}_{off,ij}(\tilde{\sigma}_{ij}(\mathbf{x}))$) capture anisotropy in stress fiber formation/disassembly rates due to stress polarization. Hence, the tensorial representation of these variables is necessary to capture the polarization in myosin motor density (and consequently stress fiber orientation) that is observed in anisotropic cellular morphologies. Furthermore, we define the cell-matrix interfacial energy $\Gamma(\Theta)$ as the sum of a) membrane/cortical tension and b) the energy of adhesions at the cell-matrix interface, where Θ is a shape factor accounting for cell elongation. Integrating the conservative energies and the energy of ATP hydrolysis over the cell volume V_c and summing it with the matrix strain energy and interfacial energy produces the generalized cell metabolic potential, R:

$$R = \int_{V_c} R_p\left(\rho_{ij}(\boldsymbol{x}), \epsilon_{ij}(\boldsymbol{x}), \Theta\right) dV_c + \int_{V_{ECM}} F_{ECM}\left(\epsilon_{ij}^{ECM}(\boldsymbol{x})\right) dV_{ECM} + \Gamma(\Theta) \quad (1)$$

where R_p is the local metabolic potential defined at every spatial coordinate $\boldsymbol{x}$ in a 3D context by summing conservative energies and the energy of ATP hydrolysis (Eq. 2 in Materials and Methods), F_{ECM} is the strain energy density of the extracellular matrix, V_{ECM} is the matrix volume and ϵ_{ij}^{ECM} is the matrix strain. The metabolic potential arises from a nonequilibrium analysis of energetic contributions governed by the kinetics of stress fiber formation and disassembly (SI Section 2.2). Similar to the 1D case, we find that the minimum metabolic potential corresponds to the steady state predicted by considering the dynamics of stress fiber formation (see SI Section 2.2.3). Hence, both the metabolic potential and the energy of ATP hydrolysis motivated here using simple physical arguments have a strong basis in nonequilibrium thermodynamics. In particular, the components of the cellular contractility and strain tensors in the steady state can be obtained from the kinetics of stress fiber assembly and the dynamics of stress fibers, as shown in SI Section 2.2.4.

Minimization of metabolic potential predicts how the shape and anisotropic contractility of metastatic cancer cells depend on collagen density

We implemented a generalized 3D model within a finite element framework to study the physical mechanisms that govern the establishment of cellular morphology, cytoskeletal contractility, and metabolism in MDA-MB-231 breast cancer cells in a three-dimensional collagen matrix. The cell body is modeled as an ellipsoidal inclusion with two semiaxes of equal radii and a third distinct radius ($a = c \neq b$), with the aspect ratio defined as $AR = {}^{a}/_{b}$ (Figure 2b). An aspect ratio of $AR = 1$ corresponds to a spherical cell, while $AR > 1$ represents elongated cells. We normalize the aspect ratio by the circularity, $\text{circ} = 4\pi \frac{\text{cross-sectional area}}{(\text{perimeter})^2}$, which is a quantity termed the elongation factor (EF) (see Figure 2b), to quantify the shape of the cells. We further assume a constant cell volume of 5000 μm^3. This is a reasonable assumption, as cell volume is regulated through water transport in and out of the cell, which requires extremely high osmotic pressures (~1 MPa)[40], approximately three orders of magnitude greater than the cytoskeletal tension observed in the cell (~1-10 kPa).

The collagen matrix is modeled as a cylinder that ensconces the cell, with a radius greater than 50 times that of the cell, to reduce boundary effects. The morphology, cytoskeletal contractility and bioenergetic requirements of cells encapsulated in a collagen matrix are tightly regulated by the density of the collagen network[16,41]. To capture this regulation, the mechanical behavior of collagen networks is described by a nonlinear fiber model[42–44] (see SI Section 2.2.5) that can represent the strain stiffening of collagen due to tension-induced realignment of collagen fibers (Figure S4b). We determine the steady-state cell shape, strain and contractility by minimizing the metabolic potential, R (Eq 1), with respect to these variables within a finite element framework (Figure S4c). This process is repeated for collagen matrices of varying densities. An iterative analysis was performed where model predictions of cell elongation and contractility at steady state were compared against corresponding experimental measurements for MDA-MB-231 cells to determine the mechanical and biophysical parameters, and the results are listed in Table S4.

Cytoskeletal stress and rates of ATP hydrolysis are higher in elongated cells. First, our model predicts that the volumetric part of the metabolic potential, υ^{cell}, which includes the mechanical, myosin binding, and ATP hydrolysis energies (Eq. 4 in Materials

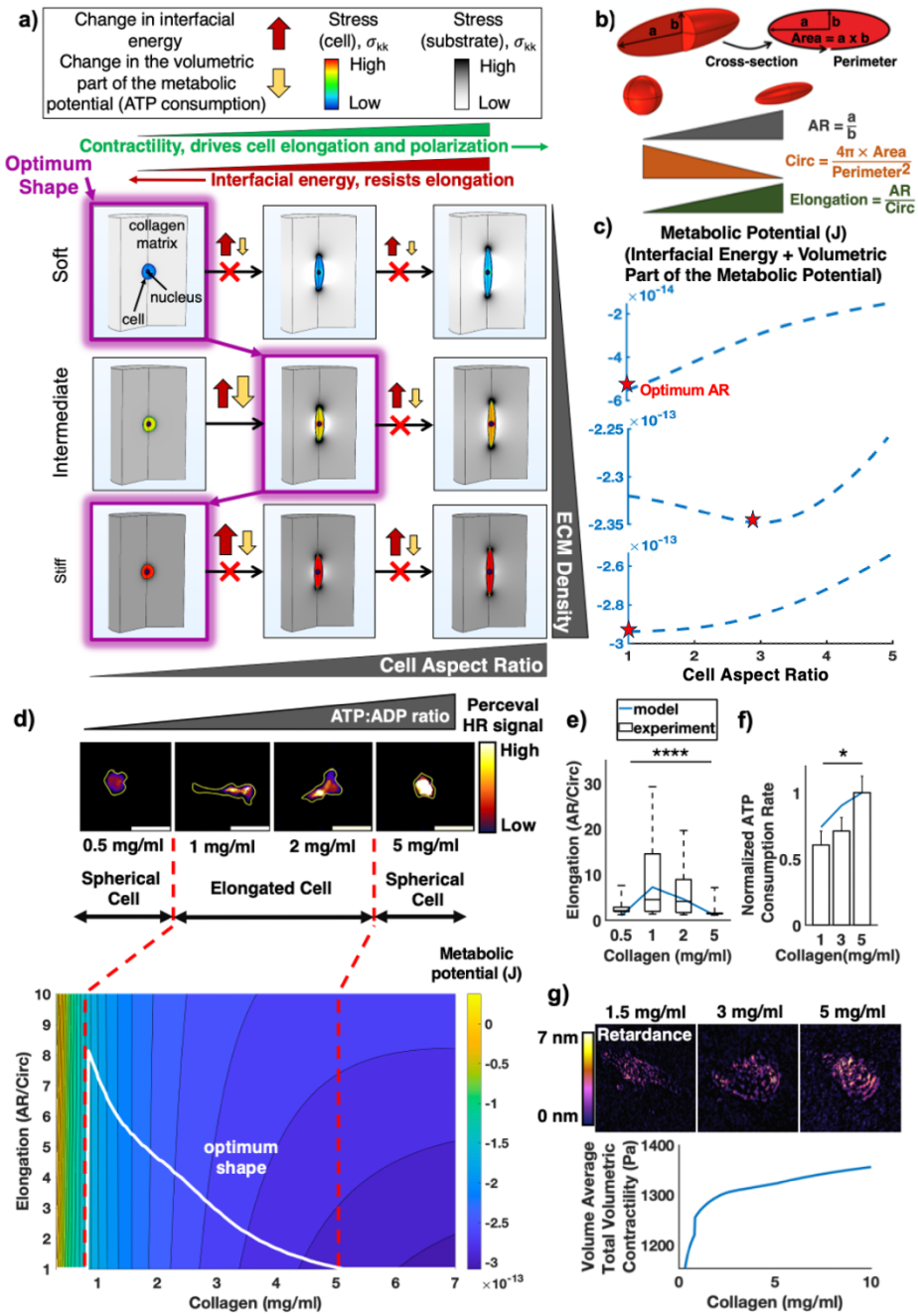

Figure 2: Minimizing the metabolic potential predicts a biphasic variation in cell shape with increasing collagen density. (a) Optimum cell shape shows a biphasic transition from spherical in low density collagen to elongated (spindle-shaped) in medium density collagen, back to spherical in high density collagen as a result of the competition between the volumetric part of the metabolic potential (red block arrows) and the interfacial energy (yellow block arrows). (b) Schematic description of cell body aspect ratio (AR), circularity (circ) and their variation with cell shape.(c) Metabolic potential as a function of cell shape for low (0.4 mg/mL), medium (2mg/mL) and high density (6 mg/mL) collagen, where the minimum in metabolic potential corresponds to the steady state optimum cell shape at all collagen densities. (d) Contour plot of the metabolic potential as a function of collagen density and cell elongation. Simulation predictions as compared to reported experimental measurements of MDA-MB-231 cells in 3D collagen for cell elongation[16] (e) and normalized ATP consumption rate[41] (f). The experimentally measured optical retardance signal[46], which correlates with contractile strain in cells is displayed in (g) along with model predictions of steady state contractility vs collagen density. Bar plots show mean ±SE, and box plots show median, 25th/75th percentiles, and 5th/95th percentiles *p<0.05, **p<0.01, ***p<0.001, ****p<0.001 with Kruskal-Wallis one-way ANOVA. Scale bar = 50 μm.

and Methods), is lower for elongated cells, as the levels of stresses are overall greater (Figure S5). At any given density of collagen, as cell elongation increases, the volume-averaged mean cytoskeletal stress ($\frac{1}{V_c}\int_0^{V_c}\frac{\sigma_{kk}}{3}dV_c$, where V_c is the cell volume) increases, saturates, and then begins to decrease at very high elongations ($EF > 50$) (see Figure S5). The initial increase occurs because isotropic contraction of an elongated cell leads to the development of an anisotropic stress field with stress concentration near the elongated ends (Figure 2a). The localized stresses at the elongated ends activate mechano-signaling pathways (Figure 1a) that upregulate stress fiber assembly and consequently ATP consumption along the elongated axis. By examining the deviatoric components of the stress, which represent the polarization of stress fibers, we find that the deviatoric stress along the elongated axis, $\tilde{\sigma}_{33}$, is indeed greater than that along the other axes (see Figure S6). In this way, the anisotropic stress field due to elongated cell morphologies leads to preferential alignment of stress fibers. Accordingly, for a given collagen density, the mean contractility $\frac{\rho_{kk}}{3}$ increases near the elongated ends (Figure S4a). As the stress generated by the initial isotropic cell contraction is greater on denser matrices, the extent of stress-regulated signaling is greater, leading to a greater density of stress fibers and consequently, for a cell of fixed elongation, greater contractility in dense collagen matrices (Figure S7). We find that the cell contractility, the energy of ATP hydrolysis and the variation in the volumetric part of the metabolic potential with cell elongation closely resemble the underlying trend in volumetric stress (Figure S8a). With increasing elongation, the volumetric stress saturates because the increase in the stress along the direction of elongation, σ_{33}, is now balanced by the decrease in stress along the other two directions, σ_{22} and σ_{11} (Figure S5). This is a consequence of the fact that the cell volume is nearly

constant, which requires that elongation along one direction be accompanied by equal levels of contraction along the other two directions.

The optimum cell aspect ratio determined by minimizing metabolic potential shows biphasic variation with collagen density. Next, we consider the effect of interfacial energy and describe the steady-state cell shape by minimizing the metabolic potential for different collagen densities. As the gel density increases, the number of ligands available increases, and the adhesive energy becomes increasingly negative, i.e., γ_1 increases for high-density collagen matrices (Figure 1c). However, as described in SI Section S2.2.6, the membrane tension is two orders of magnitude greater than the energy of receptor–ligand adhesions. Particularly, for mesenchymal cells, it has been observed that membrane tension is higher on stiffer matrices[45]. Hence, we choose the effective interfacial energy ($\gamma = \gamma_0 - \gamma_1$) to be an increasing function of collagen density, the exact functional form being determined by a sensitivity analysis (see Figure S9). When using this form for interfacial energy, the cell shape predicted by minimizing the metabolic potential shows a clear biphasic variation with matrix stiffness (see Figure 2a).

To understand how the metabolic potential dictates cell morphology, we consider the effects of cell elongation and matrix density on the volumetric part of the metabolic potential and interfacial energies separately. By examining the individual energetic components of the volumetric part of the metabolic potential, we observe that ATP hydrolysis energy is the most dominant component, as it shows the greatest change from one cell shape to another at any given matrix density (Figure S7). Thus, the shape that minimizes the volumetric part of the metabolic potential is also the one that maximizes ATP consumption and is under maximum cytoskeletal tension. The interfacial energy of the cell increases as the cell body aspect ratio increases beyond unity (Figure S10). For a given cell aspect ratio, the interfacial energy is greater for denser collagen matrices; however, the change in interfacial energy with elongation is nearly similar for all collagen densities. At low and high collagen densities, our model predicts that the cell adopts a rounded shape, while at intermediate matrix density, it has an elongated shape ($EF > 1$) (see Figure 2a), as we discuss next.

- *Low Collagen Density (<0.5 mg/ml)*: Cells in low-density collagen do not generate high magnitudes of cytoskeletal stress, even when they adopt highly elongated shapes (Figure 2a), because the surrounding matrix is too soft to support large stresses. Hence, the stress-regulated enhancement in stress fiber assembly and, consequently, the energy available through ATP hydrolysis is low for both the spheroidal and elongated configurations (Figure S7). In this case, the decrease in the volumetric part of the metabolic potential as the cell transitions from a spheroidal to an elongated shape is also very low and is not sufficient to overcome the increase in interfacial energy (Figure S10) associated with such a shape transition. Hence, our model predicts that the cell adopts a spheroidal shape (Figure 2c) in low-density collagen matrices. This finding agrees with the experimental predictions of cell elongation at low collagen densities (Figure 2d-e).
- *Medium Collagen Density (0.5–5 mg/ml):* Here, the stresses and consequently the contractility is larger for all cell elongations compared to cells in low density collagen (Figure 2a). Additionally, the decrease in the volumetric part of the metabolic potential as cell elongation changes is greater than the corresponding decrease on soft matrices (see Figure S7). This decrease is sufficient to overcome the increase in interfacial energy (Figure S10), and the cell adopts an elongated shape (Figure 2c) at steady state, which compares well with the experimentally observed cell elongation in matrices of intermediate density (Figure 2d-e).
- *High Collagen Density (>5 mg/ml):* While very high stresses and contractility are generated for cells in highly dense collagen matrices (Figure 2a), the decrease in the volumetric part of the metabolic potential with cell elongation is slightly smaller than that observed for cells in intermediately dense collagen (Figure S7). This suggests that the decrease in the volumetric part of the metabolic potential achieved with elongation saturates at intermediate values of matrix stiffness. This occurs since at high matrix stiffnesses, even spherical cells can generate high levels of stress and contractility. Thus, the associated change in the energy of ATP hydrolysis and the volumetric part of the metabolic potential with elongation is smaller for high-density collagen than for medium-density collagen. This difference indicates that interfacial energy once again prevents the cell from elongating (Figure S10). Hence, cells adopt a spherical shape on high-density collagen (Figure 2c), which has also been reported in previous studies (Figure 2d-e).

In summary, only at intermediate stiffnesses is the magnitude of contractility as well as the difference in contractility between spherical and elongated cells high enough to overcome the increase in interfacial energy, leading to elongated cell shapes at steady state. Despite the nonmonotonic variation in cell shape with collagen density, the volume-averaged cell contractility corresponding to the optimum cell shape monotonically increases with gel density (Figure 2g). The optical retardance signal obtained for MDA-MB-231 cells using quantitative polarization microscopy (QPOL)[46] is a measure of the contractile strain on actin in cells, and for MDA-MB-231 cells in 3D collagen, an increase in matrix density is associated with a greater intensity of the optical retardance signal (Figure 2g), validating our theory. Additionally, we show that the ATP consumption rate (Eq. S2.28) at steady state predicted by our model increases with collagen density (Figure 2f), which underscores that the greater contractility of cells on denser matrices is driven by their tendency to lower metabolic potential. This trend shows good agreement with the rate of ATP consumption measured experimentally for MDA-MB-231 cells as the time-averaged decrease in the PercevalHR signal after treating the cells with antimycin A and iodoacetate, which inhibit OXPHOS and glycolysis, respectively[41] (Figure 2f).

Minimizing the metabolic potential predicts two distinct morphology transitions with increasing matrix stiffness for cells on 2D substrates

We now consider the steady-state cell morphology, contractility, and ATP consumption of MDA-MB-231 cells plated on 2D PA

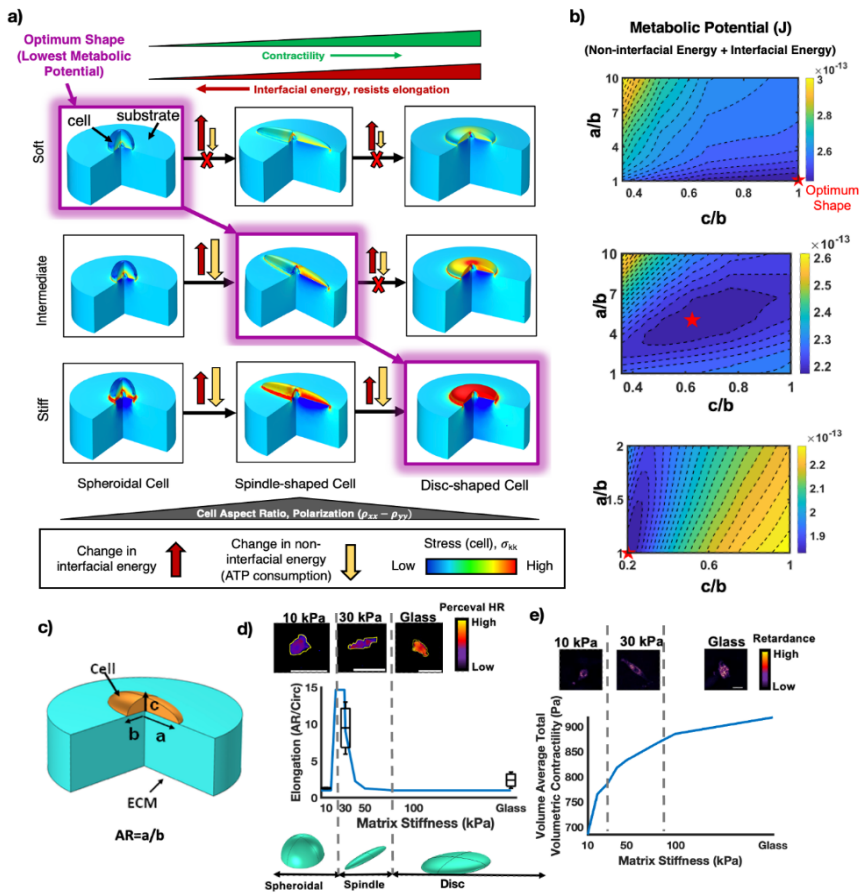

Figure 3: Minimizing the metabolic potential predicts two distinct shape transitions with matrix stiffness for cells in 2D. (a) Optimum cell shape shows a transition from hemispherical on soft gels to spindle-shaped on intermediately stiff PA gels and disc-shaped on stiff gels as determined by the interaction between the volumetric part of the metabolic potential (red block arrows) and the interfacial energy (yellow block arrows). (b) Contour plots of the metabolic potential as a function of the cell aspect ratios a/b and c/b with the optimum cell shape indicated. (c) Schematic depiction of the geometry of a cell on a 2D substrate. Comparison of (d) cell elongation and (e) cell contractility at steady state predicted by the model with the corresponding data from experiments performed with MDA-MB-231 cells seeded on unconfined 2D substrates[16,46]. Box plots show median, 25th/75th percentiles, and 5th/95th percentiles. Scale bar = 50 μm.

gels. To predict the cell shape and contractility on 2D substrates as a function of matrix stiffness, we used the biophysical parameters of MDA-MB-231 cells determined by iterative analyses performed for cells in 3D collagen (see Table S4 for description and values of parameters used) with no additional fitting parameters. Cells on 2D substrates are modeled as half-ellipsoids with distinct semiaxes, a, b and c, as shown in Figure 3c. In general, $a \neq b \neq c$, and the specific case where they are all identical represents a hemispherical cell. To completely characterize the shape of a cell seeded on 2D substrates, we define two aspect ratios, a/b and c/b, which represent elongation or contraction along the cell-matrix interface and the direction perpendicular to the cell-matrix interface, respectively (Figure 3c). The cell volume is assumed to be constant, and thus, the cell spreading area ($A = \pi ab$) scales inversely with the length of the c-axis. Thus, an increase in the cell spread area means that the cell is flattening along the c-axis. While we examined a range of cell shapes, we find that considering the energetic contributions of a particular set of three important shapes is enough to explain the morphologies adopted by cells on 2D substrates. These three shapes are a) spheroidal ($\frac{a}{b} = 1, \frac{c}{b} = 1$), (b) spindle-like ($\frac{a}{b} > 1, \frac{c}{b} < 1$) and (c) disc-like ($\frac{a}{b} = 1, \frac{c}{b} < 1$) (Figure 3a). Similar to the 3D case, the matrix is modeled as a cylinder with a radius greater than 50 times that of the cell to minimize boundary effects. The mechanical behavior of the matrix is modeled as a linear elastic matrix, which represents polyacrylamide (PA) gels[47], and the stiffness is varied from 1-200 kPa.

Unlike cells in 3D collagen networks, cells on 2D substrates have two contributions to the interfacial energy: a) cell-matrix interfacial energy γ^{CM} and b) the energy of the "free" surface of the cell $\gamma_0^c S_c$, where γ_0^c is the surface tension of the free surface of the cell (which is not in contact with the ECM); similarly, S_c is the surface area of the free surface. The cell-matrix interfacial energy, γ^{CM}, has two contributions, namely, the membrane/cortical tension associated with the cell-matrix interface γ_0^{CM} and the adhesive energy due to interactions between integrins on the cell and ligands on the matrix. γ_1^{CM}. We can write γ^{CM} as $\gamma_{eff}^{CM} S_{CM}$, where S_{CM} is the contact area at the cell-matrix interface and $\gamma_{eff}^{CM} = (\gamma_0^{CM} - \gamma_1^{CM})$ is the effective cell-substrate interfacial tension. Now, the overall interfacial energy of the cell-matrix system, Γ, can be found by summing the cell-matrix interfacial energy and the energy of the free surface. We conducted iterative analyses with simulations of MDA-MB-231 cells on 2D PA gels to determine the values of the surface tension of the free cell surface γ^C, membrane tension along the cell-matrix interface γ_0^{CM} and integrin-ligand energy γ_1^{CM} at which model predictions of cell morphology show good agreement with experimental measurements[16,46]. These values are listed in Table S4 and fall within the order of magnitude realms observed experimentally (refer SI Section 2.2.6).

To determine the steady-state cell shape as a function of matrix stiffness, we compute the metabolic potential given in Equation 1 for various cell shapes (changing $\frac{a}{b}, \frac{c}{b}$) corresponding to different values of matrix stiffness. These contours, along with the steady-state cell shape that corresponds to the minimum metabolic potential, are displayed in Figure 3a-b. While simulations have been performed over a range of matrix stiffness values, the trends

reported here for cell shape, polarization, and contractility correspond to the three representative cases of soft, intermediately stiff, and stiff matrices, which have Young's modulus values of 10, 30 and 200 kPa, respectively.

Anisotropic cell shapes develop larger cytoskeletal stress and polarized contractility. We define cell polarization as $p = (\rho_{xx} - \rho_{yy})/\rho_0$, where ρ_{xx} is the contractility along the a-axis (direction of elongation), ρ_{yy} is the contractility along the b-axis (see Figure S11a) and ρ_0 is the cell contractility in the quiescent state. As the cell shape changes from hemispheroidal to spindle, the stress field is polarized (see Figures 3a, S11c) and promotes enhanced assembly of stress fibers along the direction of elongation, which in turn increases the overall volume-averaged cytoskeletal stress $(\frac{1}{V_c}\int_{V_c}\sigma_{kk}dV_c)$ experienced by the cell (see Figure S11e) and thereby the cell contractility (Figure S11d). By examining the spatial distribution of the volumetric stress σ_{kk} along the cell body, we observe that for any gel stiffness, the model predicts the highest magnitude of stress near the cell-ECM interface for all cell shapes (Figure 3a). Consequently, the cell contractility is significantly greater near the cell-substrate interface for hemispherical, spindle and disc-shaped cells (see Figure 3a), while it is lower in regions further away from the interface that are free from constraints.

For disc-shaped cells, the stress decreases more gradually away from the cell-matrix interface than in the hemispherical and spindle-like configurations, i.e., while hemispherical and spindle-like cells can develop high magnitudes of stress only near the cell-ECM interface, and disc-shaped cells can develop more uniformly high stresses across the cell body (Figure 3a), leading to the highest overall volume-averaged cytoskeletal stress among the three configurations at all matrix stiffness levels (Figure S11e). Additionally, for all matrix stiffness values, the stress fiber density is uniformly high throughout the disc-shaped cell, leading to greater volume-averaged cell contraction (Figure S11d). As a result, the energy available through ATP hydrolysis is highest for the disc-shaped cell (see Figure S12). Similar to cells in 3D collagen, the energy of ATP hydrolysis is the most dominant component of the volumetric part of the metabolic potential, and if we disregard considerations of interfacial energy, this shape will be the optimum shape for all levels of matrix stiffness. However, by considering both the volumetric part of the metabolic potential and interfacial energies (the total metabolic potential), we find that, similar to cells in 3D collagen matrices, the optimum cell shape on a 2D substrate transitions from hemispherical on soft matrices to spindle-shaped on matrices with intermediate stiffness (Figure 3a and b).

The rationale behind the hemispherical-spindle-disc shape transition is as follows: on soft gels, although the spindle and disc-shaped cells achieve greater stress and contractility than the hemispherical cell, the associated decrease in the volumetric part of the metabolic potential is not sufficient to overcome the increase in interfacial energy (see Figure 3a). Hence, cells adopt a hemi-spherical steady-state configuration on soft substrates (see Figure 3b). On intermediately stiff gels, while the cell contractility increases significantly and is highest for the disc-like cell, it is still not high enough to overcome the high interfacial energy associated with the disc shape, and the spindle-like cell emerges as the optimum configuration (see Figure 3b). However, on stiff matrices, disc-shaped cells are able to achieve a significantly greater decrease in the volumetric part of the metabolic potential than spindle-shaped cells (Figure 3a) due to the greater extent of mechano-signaling and a lower metabolic potential, consequently emerging as the optimum cell shape (Figure 3b). Additionally, similar to cells in 3D collagen, our model predicts that steady-state contractility increases with matrix stiffness, which agrees with the experimentally measured trends in optical retardance[46], which correlates with contractile strain in actin fibers (Figure 3e). The trends in cell shape predicted by our model show good agreement with the experimental results reported for MDA-MB-231 cells (see Figure 3d) cultured on 2D PA gels. The biphasic variation in the cell aspect ratio a/b (Figure 3d) with matrix stiffness, along with the associated increase in the cell spread area (see Figure S13), fully captures the spherical spindle disc shape transition observed in cells seeded on 2D substrates. In the absence of interfacial energy, the cells adopt the shape that can achieve the maximum contractility and hence maximize ATP consumption (Figure S12b), similar to cells in 3D collagen (Figure S8b-c). Thus, the steady-state configuration adopted by cells is determined by the balance between their propensity to maximize ATP consumption and the energetic cost of adopting anisotropic shapes imposed by the interfacial energy. In the next section, we will briefly describe a model to calculate the ATP consumed by cells to maintain their steady-state configuration and how varies with stiffness.

A mathematical framework for predicting mechano-sensitive ATP replenishment

Thus far, we have shown how our model predicts that cells in stiffer environments develop more contractility and accordingly exhibit greater ATP consumption. Here, we seek to develop a theory for ATP production by cells in response to the bioenergetic demands placed on them in stiff microenvironments with the goal of quantitatively predicting important bioenergetic indicators such as ATP levels, ATP:ADP ratios, glucose uptake, and OXPHOS rates as a function of matrix stiffness. We first quantitatively describe the mechanisms that involve ATP consumption in an adherent, contractile cell in response to the microenvironment and then outline the proposed mechanosensitive ATP replenishment pathways along with a description of the model parameters that are used to quantify them (refer to SI Section 3 for full derivation and details about how the model parameters are determined).

Quantitative description of ATP consumption in stiff vs soft microenvironments: All living cells maintain a high, nonequilibrium ratio of ATP to ADP in the range of 1-10[48]. To describe ATP consumption, we consider the ATP hydrolysis reaction (see reaction (1), Table S5), where k_1^+ and k_1^- are the rate constants that govern ATP consumption and production, respectively. As ATP consumption in contractile cells is primarily due to mechanosensitive stress fiber assembly[49–51], we assume that the reaction rate constant that governs ATP consumption (k_1^+) depends on stress fiber assembly and disassembly rates, which in turn are functions of cytoskeletal stress. Therefore, we take k_1^+ to depend on the volumetric stress σ_{KK} (refer to SI Section 3 for the exact functional form). Once the tensile stress levels are known

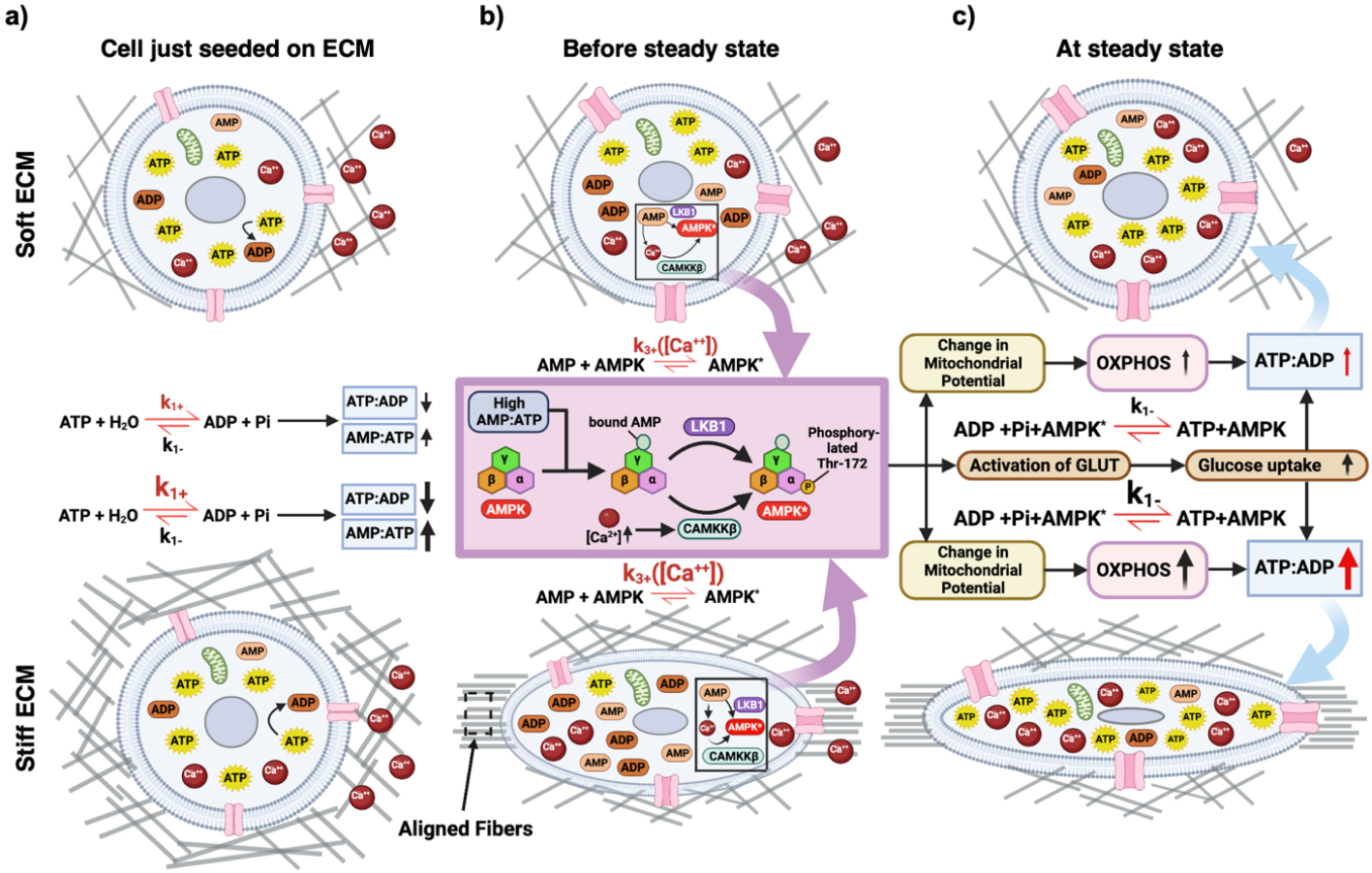

Figure 4: ATP replenishment pathway based on the mechano-sensitive calcium-mediated activation of AMPK. (a-c) Schematic representation of the ATP, ADP and AMP levels (a) immediately after the cell is seeded on the ECM, (b) before reaching steady state and (c) at steady state for cells in soft and stiff environments. The initial metabolic state just after the cell is seeded on the ECM is identical for cells in both the stiff and soft matrices, however (a), more ATP is consumed by cells on the stiff substrate due to the activation of stress-regulated signaling pathways that lead to enhanced stress fiber assembly and more ATP hydrolysis (b). Cells on stiff substrates see a marked increase in intracellular Ca^{2+} levels as compared to the baseline value due to stress-assisted opening of ion channels. Activation of AMPK is mechanosensitive and depends on intracellular Ca^{2+} concentrations (see inset purple box), leading to greater extent of AMPK activation on stiff matrices. At steady state (c), mechanosensitive activation of AMPK has upregulated ATP production such that ATP levels are higher on stiff than soft. Our model captures these mechanisms by taking the rate constant governing the reaction in which AMP and AMPK yield active AMPK, k_3^+, to depend on the intracellular calcium levels.

from the 3D active model, total ATP consumption rates can be computed by integrating the spatial consumption rates over the volume of the cell. Furthermore, considering the conversion of ADP to AMP (reaction(3), Table S5), we introduce the ratio of the reverse (k_2^+) and forward (k_2^-) reaction rate constants, γ' (Table S5), to represent this reaction. Thus, the greater cytoskeletal tension on stiff substrates and the associated ATP consumption leads to a greater decrease in the ATP:ADP ratio and an associated increase in the AMP:ATP ratio (Figure 4b) compared to those on soft substrates.

ATP replenishment through mechanosensitive calcium-mediated AMPK activation: Central to overall cellular metabolism is the "master metabolic regulator" AMPK, which regulates most of the major catabolic and anabolic pathways in cells, including OXPHOS and glycolysis, in response to changing cellular energy levels[17]. AMPK is a heterotrimer composed of the catalytic subunit AMPKα and two regulatory subunits, AMPKβ and AMPKγ. The activation of AMPK (the active form of which is referred to as AMPK*) is a critical step in the replenishment of ATP and is initiated by the allosteric binding of AMP[17] to the AMPKγ subunit. This induces a conformational change in the complex, thereby making the AMPKα subunit a more suitable site for phosphorylation by upstream kinases (Figure 4b). Two kinases, namely, LKB1 (liver kinase B1) and CAMKKβ (Ca2+/calmodulin-stimulated protein kinase kinase beta), have been shown to promote the phosphorylation of AMP-bound AMPK at Thr172 (threonine) on the AMPKα subunit (Figure 4b). Higher expression levels of these kinases lead to increased AMPK activation. We represent the formation of AMPK* by chemical reaction (4) in Table S5, such that k_3^+ denotes the rate constant that governs the activation of AMPK* and k_3^- is the reverse rate constant. Here, we consider the rate constant governing AMPK activation k_3^+ to be a function of LKB1 and intracellular calcium levels to represent the upstream effect of these kinases on AMPK activation.

As energy levels in the cell are depleted, AMP levels increase, which leads to higher levels of AMP-bound AMPK. This effect is more pronounced on stiffer substrates (Figure 4a-b). Although LKB1 levels are not known to be affected by the stiffness of the

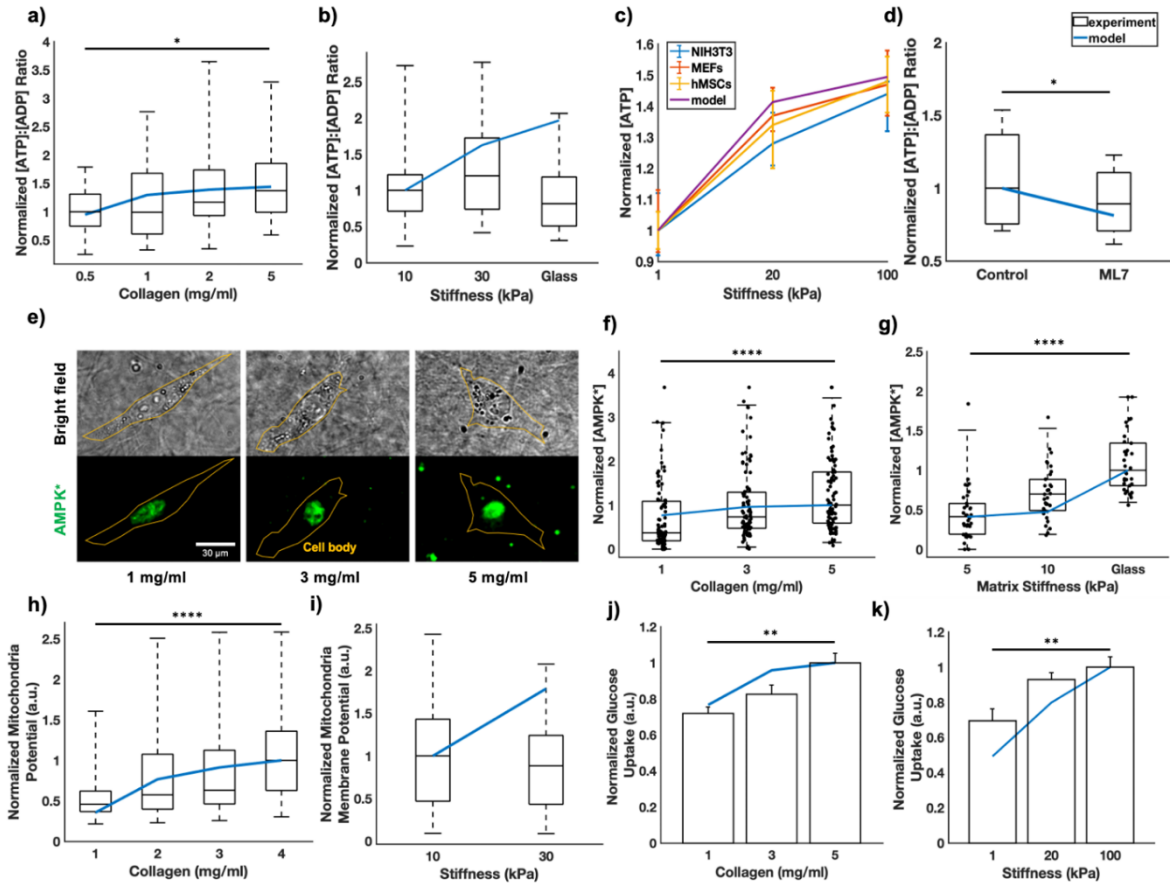

Figure 5: Model predictions of normalized ATP:ADP ratio, ATP levels, [AMPK*] levels and comparison with experimental data. (a) Least Squares fit of steady state ATP:ADP ratio vs. collagen density from theory against experimental measurements of PercevalHR signal[16] to determine model parameters. (b) Model prediction of normalized ATP:ADP ratio for MDA MB-231 cells in 2D using parameters determined from (a) compared with experimental measurements[16]. (c) Model predictions of normalized ATP levels for MDA MB-231 cells compared with experimentally measured ATP levels for hMScs, MEF and NIH3T3 cells[18]. (d) Model prediction of normalized ATP:ADP levels considering myosin recruitment rates (k_{on}) of 2.33kPa^{-1} and 1.5kPa^{-1}, the latter representing the effect of lowered myosin activity compared against experimental measurements for MDA MB-231 cells in 3D collagen of density 1.5 mg/mL treated with ML7 which inhibits MLCK and thereby, the cell's ability to generate contractile forces[41]. (e) Bright field images of MDA MB-231 cells in collagen of density 1, 3 and 5 mg/mL along with corresponding confocal microscopy images of cells stained with phosphorylated AMPK antibody. Model predictions of [AMPK*] as a function of collagen density/gel stiffness compared with experimentally measured relative levels of [AMPK*] (quantified for each cell as the total fluorescence signal using ImageJ software) for MDA MB-231 cells (f) in 3D collagen and (g) on 2D PA gels. Model predictions of [AMPK*] are compared with the reported change in mitochondrial potential for MDA MB-231 cells in (h) 3D collagen and (i) 2D PA gels[16] as well as with glucose uptake levels for MDA MB-231 cells in (j) 3D collagen[41] and (k) hMSCs on 2D gels[18]. Bar and line plots show mean ±SE, and box plots show median, 25th/75th percentiles, and 5th/95th percentiles *p<0.05, **p<0.01, ***p<0.001, ****p<0.001 with Kruskal-Wallis one-way ANOVA.

microenvironment, it is well established that intracellular calcium levels are increased on stiffer substrates in many cell types[52–54]. In particular, in mesenchymal cells, the greater membrane tension associated with stiffer microenvironments[45,55] directly leads to an increase in intracellular calcium levels through the opening of stress-activated ion channels[55,56]. This mechanosensitivity of calcium signaling is modeled by considering the reaction rate constant that governs AMPK activation, k_3^+, as an increasing function of cytoskeletal stress ($k_3^+ = k_3^+(\sigma_{kk})$). Additionally, the reverse rate constant, k_1^-, which governs ATP synthesis, is an increasing function of [AMPK*], which represents the upregulation of ATP synthesis by AMPK*. As several upstream signaling pathways mediate the activation of AMPK, it is difficult to determine the effect of cellular stress on AMPK activation through calcium signaling, and we assume that the rate constant governing AMPK activation through calcium signaling depends on cytoskeletal stress $k_3(\sigma_{KK}) = {\sigma_{KK}}^m$. The important rate constants and how they depend on various biophysical parameters are summarized in Table S5. To determine the steady-state levels of ATP, ADP and AMP, we set the rates of change in the concentration of the nucleotides to zero. Furthermore, we enforce the constraint that the total concentration of nucleotides is constant and that the sum of nonactivated and activated AMPK is also a constant. This leads to a set of five equations that we solve simultaneously to determine the concentrations of phosphates and the two forms of AMPK at steady state (refer to SI Section 3.1 for a detailed derivation).

Cells maintain higher ATP:ADP ratios and activated AMPK in stiffer microenvironments

Our theory captures the experimentally observed trend that ATP:ADP increases with increasing collagen density (Figure 5a).

We performed a least-squares fitting of Eq. (S3.17) to the experimentally measured ATP:ADP ratios for collagen densities from 0.5 to 5 mg/mL to determine the model parameters (Table S6, Figure S14). To validate the model, we analyzed MDA-MB-231 cells in 2D microenvironments using the same parameter values as listed in Table S6, with n being adjusted to a slightly lower value (see SI Section 3.1). The steady-state ATP:ADP ratio for MDA-MB-231 cells on 2D PA gels predicted from our theory shows a monotonic increase with matrix stiffness (Figure 5b), in agreement with experimental measurements of MDA-MB-231 cells plated on PA gels[16]. Despite cell polarization showing biphasic variation with increasing matrix stiffness, unlike in the case of 3D collagen, the steady-state ATP:ADP ratio shows a monotonic increase in both 2D and 3D microenvironments, as the optimum configuration adopted by cells on stiff substrates has increased contractility (Figure 2g and 3e), leading to both increased ATP consumption and associated replenishment on stiff substrates.

Model predictions of activated AMPK levels increase with ECM stiffness and correlate with experimentally measured levels of glucose uptake and OXPHOS. Our theory provides a general framework to predict important biophysical parameters and variables, key among which are activated AMPK levels as a function of matrix stiffness. As experimental data pertaining to the direct measurement of [AMPK*] at the single-cell level is not available, we performed experiments to measure [AMPK*] at the single-cell level in cells cultured on both 2D PA gels and in 3D collagen (Figure 5f and 5g). The total immunofluorescence signal calculated from confocal images of MDA-MB-231 cells stained for AMPK phosphorylated at αThr172 was used to quantify the relative amount of activated AMPK (refer to SI Section 3.2 for details). We found significant increases in AMPK activation in stiffer environments both in 3D collagen (Figure 5f) and on 2D PA gels (Figure 5g), in good agreement with the increase in activation predicted by our model (see SI Section 3.4). These findings are also consistent with other reports in the literature that revealed elevated AMPK activation in response to stiffer substrates on both short (~5 hrs) and long (~24 hrs) culture timescales[18]. Furthermore, we observe strong localization of activated AMPK to the nucleus (Figure 5e), which is consistent with its known role as a transcription factor[57,58]. We also find that our model predictions of increased AMPK activation in stiffer microenvironments strongly correlate with increased glucose uptake (Figure 5j-k) and changes in mitochondrial potential (an indicator of increased OXPHOS rates in cell mitochondria) (Figure 5h-i), as measured experimentally in mesenchymal cells[16,41] in both 2D and 3D microenvironments. To further assess the ability of our model, we compared the model predictions of the steady-state ATP levels on 2D PA gels to experimental measurements for other mechanosensitive cell types. We find that our model prediction of the change in ATP (and hence glucose uptake) with matrix stiffness is representative of cell metabolism across various mesenchymal cell types (Figure 5c)[18].

Pharmacological inhibition of myosin activity leads to decreased steady-state ATP:ADP ratios. To directly predict the effect of inhibiting myosin activity in our model, we simulated MDA-MB-231 cells in 3D collagen with reduced sensitivity to stress by choosing a smaller value for the kinetic constant governing stress fiber assembly k_{on} while maintaining the other biophysical

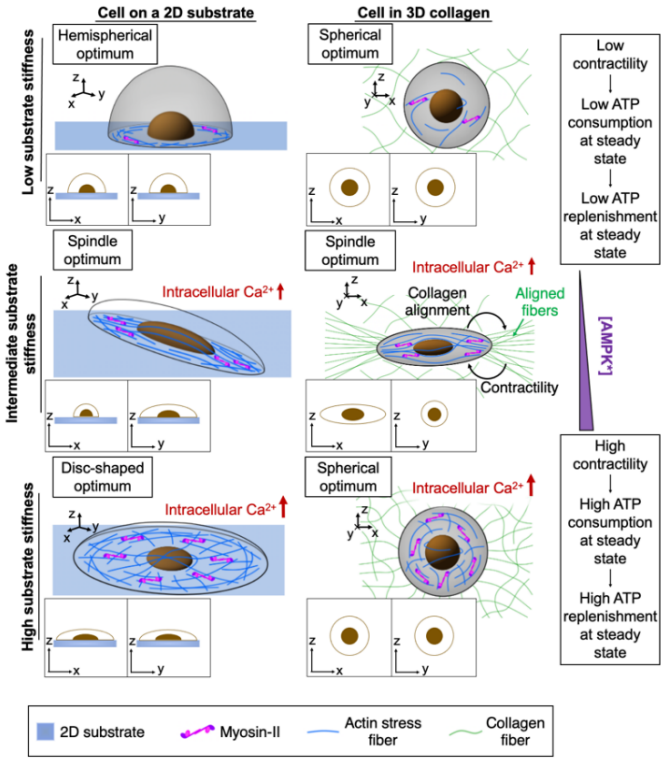

Figure 6: A model to predict how cell shape, contractility, and metabolism depend on mechanosensitive stress fiber assembly in adherent cells. Cell shape and ECM stiffness determine the distribution and magnitude of stresses generated in an adherent cell which, through mechanosensitive pathways, regulate the establishment of stress fibers. The decrease in energy achieved by coupling the ATP hydrolysis with stress fiber assembly drives the cell towards a more contractile state and to adopt morphologies that maximize ATP consumption and minimize interfacial energy. Simultaneously, the same mechanosensitive pathways upregulate cytosolic calcium levels which leads to the activation of AMPK through a calmodulin mediated pathway, replenishing cellular ATP stores.

constants at the same values listed in Table S4. A smaller value of k_{on} means that stress fiber formation rates are lower, even in dense collagen gels, which results in lower levels of cytoskeletal stress (Figure S15). Thus, the rate constant governing ATP consumption k_1^+, which depends on cytoskeletal stress (Table S5), is now smaller, leading to lower ATP consumption. Furthermore, since stress-regulated intracellular calcium levels are also lower, the reaction rate constant governing AMPK activation k_3 is also now smaller, and our theory predicts a lower extent of ATP replenishment. Hence, we expect the steady-state ATP:ADP ratio to be smaller for this case. We considered a collagen density of 1.5 mg/mL in our simulations, which represents gels of intermediate stiffness. For the same gel density, the contractility, which correlates with the number density of engaged motors, is lower, leading to overall lower cytoskeletal tension. Using Eq. (S3.17), we predict that the steady-state ATP:ADP ratio for the cells with a reduced k_{on} is smaller (Figure 5d). The inhibition of myosin light chain activity (MLCK) by treating MDA-MB-231 cells in 3D collagen (density of 1.5 mg/mL) with ML7 is reported to have a similar effect, and our model predictions show good agreement with the ATP:ADP ratio measured after inhibition using PercevalHR[41] (Figure 5d).

ATP:ADP ratio and OXPHOS rate is higher for more elongated cells and cells with a larger spread area on 2D substrates

Next, we predicted the normalized ATP:ADP ratio as previously measured in MDA-MB-231 cells cultured on 2D micropatterned PA gels[16]. By tailoring the micropattern, cells can be confined to a predetermined fixed area or can be forced to adopt increasingly elongated aspect ratios. For both cases, the cellular energy level as a function of cell elongation and spread area was measured by using the PercevalHR ratiometric reporter to measure the ATP:ADP ratio. On PA gels with stiffnesses of 10 and 30 kPa, we consider a) cells with a fixed elongation ($AR/circ \sim 1$) and (b) cells with a fixed area, where the ATP:ADP ratio as a function of increasing cell spread area or cell elongation are computed. To model confined cell spreading, we considered MDA-MB-231 cells (properties listed in Table S4) on rectangular micropatterns with side lengths a and b. First, by holding the cell elongation fixed at unity, we vary the rectangular micropattern area and determine the steady-state cell contractility, strain and cytoskeletal stress by solving Equations S2.17a-b at every integration point (see SI Section 3.4.4 for details). Then, we determine the volume-averaged cytoskeletal stress $\frac{1}{V_c}\int_0^{V_c} \sigma_{kk}\, dV_c$ as a function of the cell spread area and use it to determine the steady-state ATP:ADP ratio (Eq. S3.17) as a function of the cell spread area (model parameters used are the same as determined by fitting data for cells in 3D collagen and are listed in Table S6).

Our model predicts that with increasing cell spreading area (while holding the elongation constant), the ATP:ADP ratio increases (Figure S16a). To understand the rationale behind this, let us denote the stress components along the base lengths a and b as σ_a and σ_b, respectively. Micropatterns that confine cell elongation can be thought of as restricting the cell to shapes that are more hemispherical in nature, and as the cell spread area increases, there is equiaxial recruitment of myosin motors along both base lengths a and b, leading to a greater increase in stress, i.e., both σ_a and σ_b increase by the same levels (as the cell area increases) and remain equal in magnitude ($\sigma_a = \sigma_b$), contributing equally to the overall increase in volumetric cytoskeletal stress σ_{kk}. This is associated with increased ATP consumption and consequent replenishment (Figure S16a). In contrast, for cells confined to a fixed area, more stress fibers preferentially assemble along the elongated axis (a), leading to greater stress in the direction of elongation, i.e., $\sigma_a > \sigma_b$, and a consequent increase in ATP consumption and replenishment. Accordingly, our model predicts that the ATP:ADP ratio increases with cell elongation (Figure S17a). Furthermore, for the same increase in elongation, cells on stiffer matrices achieved a greater steady-state ATP:ADP ratio (Figure S17a) due to the additional effect of increased substrate stiffness, which promoted the development of greater cytoskeletal stress and increased activation of mechanosensitive pathways that upregulated contractility. We also compare model predictions of the extent of AMPK activation that occurs when cells are allowed to elongate or experimentally measured mitochondrial membrane potentials (Figure S17b). Our model predicts that the concentration of activated AMPK will increase with both spread area (Figure S16b) and cell elongation (Figure S17b) owing to increased signaling due to enhanced contractility in both scenarios. All these model predictions show good agreement with experimental results reported for MDA-MB-231 cells[16] (Figure S17a-b) and serve to further validate the proposed model for ATP replenishment in a context where cell activities other than the establishment of long-term contractility, such as migration, cannot contribute to the observed differences in energy levels.

Discussion

In this study, we developed a nonequilibrium chemo-mechanical model for adherent cells and elucidated the role of mechanosensitive signaling in cell metabolism and changes in morphology and contractility in response to the stiffness of the extracellular microenvironment (Figure 6). We propose the concept of a "metabolic potential" as the sum of energies associated with the establishment of cell contractility, namely, the myosin binding energy, motor work, strain energy, energy of ATP hydrolysis, and cell-matrix interfacial energy (Figure 1b), and we demonstrate that the contractility and strain fields generated by minimizing this metabolic potential are equivalent to the steady-state fields predicted by considering the kinetics of mechanosensitive stress fiber assembly (SI Section 2), which is consistent with the Second Law of Thermodynamics. Therefore, we predict the steady-state cell shape and contractility of MDA-MB-231 cells (i) encapsulated in 3D collagen and (ii) seeded on 2D PA gels as a function of matrix stiffness by minimizing metabolic potential with respect to contractility, strain, and cell elongation. For both of these cases, we showed that elongated cells display more contractility and polarized stress fiber formation, leading to decreased metabolic potential, while the interfacial energy between the cell membrane and matrix increases with cell elongation and penalizes anisotropic cell shapes. The interplay between these competing energies leads to the formation of a minimum metabolic potential of the cell, which we identify as the optimum shape of the cell body. Specifically, our model reveals that cells in 3D collagen show a biphasic variation in elongation with increasing collagen density from spherical to elongated and then back to spherical (Figure 2a), while cells on 2D substrates displayed similar nonmonotonic variation with increasing matrix stiffness from hemispherical to spindle to disc-like shapes (Figure 3c). However, the steady-state configuration predicted by our model is always more contractile in stiffer environments.

We show that our predictions agree with the cell body shapes reported for MDA-MB-231 cells as a function of collagen density (Figure 2d-e) and PA gel stiffness (Figure 3d)[16] as well as with similar observations reported for fibroblasts[59]. In addition, increased fiber alignment was observed in highly dense collagen matrices[44,60,] suggesting significant matrix remodeling activity, which further reinforces the idea that cells are, in fact, highly contractile on stiff substrates. However, it should be noted that when cells lack the ability to degrade the matrix, cellular traction, contractility, and adhesion formation are suppressed, as reported for hMScs encapsulated in covalently crosslinked hydrogels[61]. This same phenomenon may be observed for MDA-MB-231 cells in very high-density collagen matrices but likely will not play a role in the observed cell behavior at the intermediate collagen densities considered here ($\leq$ 6 mg/ml). Furthermore, our model predicts that the deformation energy stored in the collagen matrix due to contractile forces exerted by MDA-MB-231 cells is on the order of 0.03-0.07 pJ, which is in good agreement with

experimental measurements of the strain energy of these cells measured as the deformation energy released 30 min after treatment with cytochalasin D[62] (Figure S18a). On 2D gels, the predicted strain energy is on the order of 0.002 pJ (on PA gels of stiffness 20kPa) which is also in good agreement with experimental measurements made using traction force microscopy of rat embryonic fibroblasts (REFs)[63] (Figure S18b). To understand why the strain energy of linear elastic PA gels is lower than that of collagen gels, we consider that collagen fibers stiffen along the direction of applied principal tensile stretch[44,] which can facilitate long-range force transmission in nonlinearly elastic matrices. For a cell contracting in a fibrous matrix, the force in the matrix was found to persist at distances that were several times the cell diameter[44,64], and this larger interaction field could account for the greater matrix strain energy experienced in 3D collagen matrices than that experienced in PA gels.

Importantly, we also present a model for ATP replenishment based on mechanosensitive activation of AMPK that can predict the steady-state levels of ATP, ADP, and activated AMPK as a function of cytoskeletal stress or matrix stiffness (Figure 4). It has been reported using PercevalHR measurements that the ATP:ADP ratio of fully spread cells is greater in stiff environments, as is cell glucose uptake and mitochondrial potential[16,41], suggesting that ATP replenishment through OXPHOS and glycolysis is important for establishing and maintaining cytoskeletal contractility and is modulated by the mechanical properties of the cell microenvironment. We show that our model can capture these reported trends for cells in both 3D (Figure 5a) and 2D (Figure 5b) environments and predict a steady-state ATP:ADP ratio that increases with matrix stiffness. Furthermore, our model can predict experimentally observed increases in the ATP:ADP ratio with cell elongation and spread area in cells seeded on micropatterned PA gels (Figures S16, S17). Hence, the model accurately predicts that the cell tailors its energy production to meet the energy demands imposed on it due to cytoskeletal reorganization in different environments. Note we assume that the differences in ATP consumption and hence in AMPK activation between the stiff and soft systems are chiefly due to differences in cytoskeletal contractility. This idea is reinforced by experiments in which pharmacological inhibition of myosin light chain (MLC) kinase led to a decreased ATP:ADP ratio, suggesting decreased AMPK activation[41]. This correlates with our model predictions (Figure 5d) using suppressed kinetic parameters, further reinforcing the idea that as contractility is inhibited, the cell's energy demands are lower, and hence, energy replenishment pathways are not triggered.

An interesting aspect of our model is that, as we have shown in Supplementary Section 2.2.3, all the energy from ATP consumed at steady state is dissipated as heat. As there is no net addition of stress fibers at steady state and consequently no change in the conservative energy of the cell, the steady state rate of heat dissipation (Eq. (S2.28)) is a measure of the maximum power that can be generated by the cell. We may therefore calculate the steady-state power for a cell encapsulated in a collagen matrix with a density of 0.82 mg/mL (which is representative of physiological ECM stiffness). This value is found to be 0.4 fW (considering a cell volume of 5000 μm^3, as listed in Table S4), while similar calculations for cells on a PA gel with a stiffness of 10 kPa yield approximately 0.3 fW (see Table S2 for a list of parameter values used to determine the cell power). Since 1 femtowatt of power is roughly equivalent to 20,000 ATP molecules consumed per second[59], we predict that ~8000 ATP molecules are consumed by the cell per second to maintain its steady-state configuration. The power generated by myoblasts is in the range of 0.1-0.5 fW, as determined by measuring the force these cells exert against a deformable plate and the velocity of shortening of the cell[36]. This provides an estimate of the mechanical power as the cell contracts and shows good agreement with our model predictions of cells in 3D collagen gel. Furthermore, we find that cells in low -density collagen (~0.5 mg/mL) dissipate only 0.26 fW, approximately 30% less than the power generated on high-density collagen (0.4 fW in 0.82 mg/mL), reinforcing the idea that cells consume more ATP on stiffer/denser matrices.

Understanding the role of mechanical cues in modulating energy production has important implications, particularly for the metastasis of cancer cells. It has been shown that, depending on the stiffness of the microenvironment, either OXPHOS or glycolysis can play an essential role in promoting tumor metastasis and membrane activity in cancer cells. Hence, it is vital to assess how matrix stiffness affects energy production in cells. Although we have restricted our attention in this study to predicting the steady-state energetics of cells in response to matrix stiffness, the ideas presented here can be extended to dynamic processes such as cell spreading and migration, which will be the focus of future work.

Materials and Methods

A 3D chemo-mechanical formulation of the metabolic potential

Here, we briefly describe (refer to SI Section 2 for details) a general 3D model for a contractile cell to describe the effect of stress-activated signaling pathways on the metabolic budget of the cell. The key mechanical components of this model are a) stress fibers composed of active contractile elements in parallel with passive components representing the cell cytoskeleton, b) a poroelastic nucleus, c) adhesions that provide a mechanical connection between the cell and microenvironment and d) the extracellular matrix or substrate.

<u>*A) Stress fibers*</u>: In the 3D model, we treat the contractility, stress, and strain fields as tensor variables. This is because the cell can adapt to nonspherical shapes that generate spatially nonuniform anisotropic stresses, and motors can be polarized or oriented in different directions at a given location in the cell (Figure S4a). In this case, the contractility fields (motor densities associated with stress fibers) are anisotropic, i.e., $\rho_{11} \neq \rho_{22} \neq \rho_{33}$, as are the stresses. Additionally, the stresses and contractility can vary spatially across the cell body; hence, we consider these quantities to depend on the spatial coordinates, $\mathbf{x}$. The volumetric part of the contractility tensor $\rho_{kk}(\mathbf{x}) = (\rho_{11}(\mathbf{x}) + \rho_{22}(\mathbf{x}) + \rho_{33}(\mathbf{x}))/3$ represents the cell contraction averaged over all directions and hence is a measure of the density of stress fibers per unit volume (Figure 3a), where $\mathbf{x}$ denotes the spatial coordinates in the cell. The deviatoric part of the contractility, $\tilde{\rho}_{ij}(\mathbf{x}) = \rho_{ij}(\mathbf{x}) - (1/3)\rho_{kk}(\mathbf{x})\delta_{ij}$, is a measure of the deviation of each component of contractility from the mean and can be considered to represent

the extent of polarization of motors or actin stress fibers. We define the conservative energy densities, namely, the myosin binding energy (Eq. S2.8), motor work (Eq. S2.9) and strain energy of the passive components (Eq. S2.10)), at every point in the cell. To describe the effect of mechanotransductive pathways on myosin motor activity and ATP consumption, we defined the rate parameters governing stress fiber assembly $k_{on_{ij}}$ and disassembly $k_{off_{ij}}$, which are anisotropic tensor quantities (refer to SI Section 2.2 for tensorial description of the energies). The on- and off-rates can further be decomposed into volumetric and deviatoric parts (Eqs. S2.12b, c), the volumetric parts of which ($k_{on}^{v}(\sigma_{kk}(\mathbf{x}))$ and $k_{off}^{v}(\sigma_{kk}(\mathbf{x}))$) capture the overall change in stress fiber assembly rates dependent on the mean stress (i.e., $k_{on}^{v}(\sigma_{kk}(\mathbf{x})) = \left(k_{on,11}(\sigma_{kk}(\mathbf{x})) + k_{on,22}(\sigma_{kk}(\mathbf{x})) + k_{on,33}(\sigma_{kk}(\mathbf{x}))\right)/3$), and the deviatoric parts of which ($\tilde{k}_{on,ij}(\tilde{\sigma}_{ij}(\mathbf{x}))$ and $\tilde{k}_{off,ij}(\tilde{\sigma}_{ij}(\mathbf{x}))$) capture anisotropy in fiber assembly kinetics due to stress polarization. We adopted this tensorial implementation for stress fiber assembly and disassembly rates because the overall alignment and assembly of stress fibers are influenced by cytoskeletal stress. For example, stress fiber formation was found to increase with the rigidity of the microenvironment in both mesenchymal and endothelial cells[65], and overall alignment is highly dependent on cell shape[66]. By considering the kinetics of stress fiber formation and disassembly, we formulate an expression for the energy of ATP hydrolysis (see Eq. S2.12a) in terms of the rate parameters governing stress fiber assembly $k_{on_{ij}}$ and disassembly $k_{off_{\mathrm{ij}}}$ as:

$$F_{ATP} = \underbrace{-\frac{1}{3}\frac{k_{on}^{v}\left(\sigma_{kk}^{cell}(\boldsymbol{x})\right)}{k_{off}^{v}\left(\sigma_{kk}^{cell}(\boldsymbol{x})\right) + k_{on}^{v}\left(\sigma_{kk}^{cell}(\boldsymbol{x})\right)}\frac{\Delta G}{\rho_0}\rho_{kk}(\boldsymbol{x})}_{ATP\ hydrolysis\ energy\ due\ to\ motor\ recruitment} \underbrace{-\sum_{i=1}^{3}\sum_{j=1}^{3}\frac{\tilde{k}_{on,ij}\left(\tilde{\sigma}_{ij}(\boldsymbol{x})\right)}{\tilde{k}_{off,ij}\left(\tilde{\sigma}_{ij}(\boldsymbol{x})\right) + \tilde{k}_{on,ij}\left(\tilde{\sigma}_{ij}(\boldsymbol{x})\right)}\frac{\Delta G}{\rho_0}\tilde{\rho}_{ij}(\boldsymbol{x})}_{ATP\ hydrolysis\ energy\ due\ to\ cell\ polarization} \quad (2)$$

The specific functional dependence of the on and off rates on stress that we use is given in Eq. S2.31, and the resulting form for the energy available through ATP hydrolysis is given in Eq. S2.30. Physically, this formulation captures the fact that ATP hydrolysis is energetically downhill and can drive otherwise unfavorable processes such as myosin binding and straining of the cytoskeleton and matrix described here. However, since the release of this energy is directly tied to the mechanosensitive activity of myosin motors in stress fibers, the kinetics of stress-dependent signaling pathways regulate the rate at which this process can occur. We incorporate this aspect by making $k_{on_{ij}}$ an increasing function of stress (σ_{ij}) and $k_{off_{ij}}$ a decreasing function of stress. When the cell experiences high levels of cytoskeletal tension (e.g., on stiff substrates), the energy available from ATP consumption increases as the rate of myosin motor engagement and the time over which motors remain bound increase.

B) Adhesions at the cell-matrix interface: Transmembrane proteins at the cell-ECM interface, such as integrins, form a bond with ligands on the ECM and play an important role in transmitting forces to the cell cytoskeleton. To capture the cellular morphology in 2D and 3D microenvironments, we also introduce an interfacial energy, Γ, which is a function of the cell shape. There are two contributions to the interfacial energy: the cell surface tension, γ_0, which resists any increase in the cell area or elongation, and an adhesive contribution from membrane protein–ligand interactions, γ_1 which favors an increase in the cell surface area along the cell-matrix interface (Figure 1c). Cell membranes consist of lipid bilayers tethered to an underlying rigid actin–myosin cortex. Hence, any change in the cell membrane area is accompanied by unfavorable stretching of membrane-engaged proteins that resist expansion in the cell area as well as by sustained contraction of the underlying actomyosin cortex. We consider these effects to represent the energetic cost of stretching the cell membrane. The adhesive element represents the reduction in energy achieved due to bond formation between receptors such as integrin at the cell-matrix interface and ligands present in the matrix. The relative strengths of these two quantities determine whether the total interfacial energy $\Gamma = \left((\gamma_0 - \gamma_1)S\right)$ will increase or decrease with cell surface area, S (Figure 1c). An equation to estimate the adhesive energy is presented in SI Section 2.2.6 (Eq. S2.39)), and a rough estimate of the receptor–ligand energy is found to be on the order of $\sim 10^{-6} N/m$. The typical membrane tension values[67] for the cell are on the order of $\sim 10^{-4} - 10^{-5} N/m$; therefore, we consider the effective interfacial energy to be a positive quantity that increases with cell surface area. Likewise, we account for changes in membrane tension and adhesive energy with changing ECM ligand density, as explained further in SI Section 2.2.6. 44 In our coarse-grained approach, we treat the receptor–ligand bond as an elastic layer with mechanical properties $E_{integrin}$ and $\nu_{integrin}$, which represent the effective Young's modulus and Poisson's ratio, respectively (Table S4).

C) The nucleus: We assume that the viscous relaxation of the nucleus is negligible (see SI Section 2.1.2) and model the nucleus as a linear elastic spheroidal inclusion encapsulated within the cell with elastic properties K_{nuc} and μ_{nuc} denoting its bulk and shear modulus, respectively. Transmission of force from the cytoskeleton to the nuclear envelope is facilitated by LINC complex proteins[68–70] and to account for effective force transmission to the nucleus, we model these linker proteins as a softer thin, elastic layer around the nucleus.

D) Mechanical response of the microenvironment: We consider two types of cell microenvironments in this work: 1) cells encapsulated in 3D collagen and 2) cells seeded on 2D PA gels. Following our previous work, the mechanical behavior of collagen is described using a fibrous nonlinear constitutive model that captures the strain-stiffening effect of fiber alignment under tension[44] (see SI Section 2.2.5). The bulk and shear moduli of collagen as a function of its density were determined from experimental measurements of the equilibrium modulus of collagen gels[16]. 2D PA gel substrates are modeled as linear elastic, as AFM measurements have shown that gels with stiffness values of physio-pathological relevance exhibit ideal linear elastic behavior even at the nanometer scale[47].

Generalized 3D expression for the metabolic potential of an adherent cell

We define the local metabolic potential R_p at every spatial coordinate $\boldsymbol{x}$ in a 3D context by summing all energetic contributions, namely, (a) the conservative energy density F_c, which is composed of the myosin binding, motor work and strain energy densities of passive components, namely, the cytoskeleton and the nucleus, and (b) the energy from ATP hydrolysis per unit volume, which can be decomposed into volumetric and deviatoric parts as:

$$\begin{aligned} &R_p\left(\rho_{ij}(\boldsymbol{x}),\epsilon_{ij}(\boldsymbol{x}),\Theta\right) \\ &= \underbrace{F_c\left(\rho_{ij}(\boldsymbol{x}),\epsilon_{ij}(\boldsymbol{x}),\Theta\right)}_{\text{Conservative contributions}} \\ &\underbrace{-\frac{1}{3}\frac{k_{on}^{v}\left(\sigma_{kk}^{cell}(\boldsymbol{x})\right)}{k_{off}^{v}\left(\sigma_{kk}^{cell}(\boldsymbol{x})\right)+k_{on}^{v}\left(\sigma_{kk}^{cell}(\boldsymbol{x})\right)}\frac{\Delta G}{\rho_0}\rho_{kk}(\boldsymbol{x})}_{ATP\ hydrolysis\ energy\ due\ to\ motor\ recruitment} \\ &\underbrace{-\sum_{i=1}^{3}\sum_{j=1}^{3}\frac{\tilde{k}_{on,ij}\left(\tilde{\sigma}_{ij}(\boldsymbol{x})\right)}{\tilde{k}_{off,ij}\left(\tilde{\sigma}_{ij}(\boldsymbol{x})\right)+\tilde{k}_{on,ij}\left(\tilde{\sigma}_{ij}(\boldsymbol{x})\right)}\frac{\Delta G}{\rho_0}\tilde{\rho}_{ij}(\boldsymbol{x})}_{ATP\ hydrolysis\ energy\ due\ to\ cell\ polarization} \end{aligned} \quad (3)$$

where Θ is a variable containing information about the cell shape, for example, the aspect ratio of an elongated cell. We note that R_p is a functional quantity due to the spatial dependence of $\rho_{ij}(\boldsymbol{x})$ and $\epsilon_{ij}(\boldsymbol{x})$ and, as such, requires a functional derivative to minimize with respect to these quantities. Next, we can define the metabolic potential by integrating the local metabolic potential over the cell volume and adding the interfacial energy along with the matrix strain energy (see Eq. 1). The metabolic potential of a cell represents the potential of a cell to enhance its contractility and alter its morphology/shape in response to the mechanical properties of its microenvironment by considering mechanosensitive cytoskeletal kinetics. Furthermore, we define the volumetric part of the metabolic potential as the sum of the conservative and ATP energy densities integrated over the cell volume plus the conservative strain energy of the extracellular matrix, i.e.,

$$\upsilon^{cell} = \int_{V_c}\left(F_c + F_{ATP}\right)dV_c + \int_{V_{ECM}} F_{ECM}\,dV_{ECM} \quad (4)$$

As in the micropost example, the minimization of the metabolic potential with respect to the contractility, strain, and shape yields the rate of ATP consumption in the cell at steady state (Eq. S2.29).

To determine the optimum cell shape and contractility as a function of matrix stiffness, we employed a finite element procedure, as described in SI Section 2.3 (Figure S4c). Briefly, we construct cell geometries with varying cell body aspect ratios and discretize the geometry within a finite element framework. At every spatial coordinate $\boldsymbol{x}$, we determine the steady-state cellular contractility and strain by minimizing the local metabolic potential R_p with respect to $\rho_{ij}(\boldsymbol{x})$ and $\epsilon_{ij}(\boldsymbol{x})$ by taking functional derivatives of R_p with respect to these variables. This yields a set of partial differential equations that we solve for a given cell body aspect ratio (Eqs. S2.17a-b). Then, knowing the spatial variation of the contractility and strain, we determine the cell metabolic potential R corresponding to a particular cell body aspect ratio by summing the local metabolic potential R_p integrated over the cell volume with the interfacial energy corresponding to that shape (Eq. 1). This process is repeated for different cell body aspect ratios, and the optimum cell shape is identified as the cell body aspect ratio that has minimum metabolic potential. We repeated this procedure for different matrix stiffness values to generate the observed variations in the optimum cell shape and contractility with stiffness.

Acknowledgements

The authors gratefully acknowledge the assistance of Elena Sorokina (University of Pennsylvania) in preparing 3D collagen cultures. This work was supported by NIH Award U54CA261694 (V.B.S.); NCI Awards R01CA232256 (V.B.S.); NSF CEMB Grant CMMI-154857 (V.B.S.); NSF Grants MRSEC/DMR-1720530 and DMS-1953572 (V.B.S.); NIBIB Awards R01EB017753 and R01EB030876 (V.B.S.).

References

1. Discher, D. E., Janmey, P. & Wang, Y. Tissue Cells Feel and Respond to the Stiffness of Their Substrate. *Science (1979)* **310**, 1139–1143 (2005).
2. Nagayama, M., Haga, H., Takahashi, M., Saitoh, T. & Kawabata, K. Contribution of cellular contractility to spatial and temporal variations in cellular stiffness. *Exp Cell Res* **300**, 396–405 (2004).
3. Jain, N., Iyer, K. V., Kumar, A. & Shivashankar, G. V. Cell geometric constraints induce modular gene-expression patterns via redistribution of HDAC3 regulated by actomyosin contractility. *Proc Natl Acad Sci U S A* **110**, 11349–11354 (2013).
4. Sonam, S., Sathe, S. R., Yim, E. K. F., Sheetz, M. P. & Lim, C. T. Cell contractility arising from topography and shear flow determines human mesenchymal stem cell fate. *Sci Rep* **6**, 1–12 (2016).
5. Griffin, M. A., Sen, S., Sweeney, H. L. & Discher, D. E. Adhesion-contractile balance in myocyte differentiation. *J Cell Sci* **117**, 5855–5863 (2004).
6. Park, J. S. *et al.* Mechanical regulation of glycolysis via cytoskeleton architecture. *Nature* **578**, 621–626 (2020).
7. Kusakabe, T., Motoki, K. & Hori, K. Mode of Interactions of Human Aldolase Isozymes with Cytoskeletons. *Arch Biochem Biophys* **344**, 184–193 (1997).
8. Wang, J., Morris, A. J., Tolan, D. R. & Pagliaro, L. The molecular nature of the F-actin binding activity of aldolase revealed with site-directed mutants. *Journal of Biological Chemistry* **271**, 6861–6865 (1996).
9. Hu, H. *et al.* Phosphoinositide 3-Kinase Regulates Glycolysis through Mobilization of Aldolase from the Actin Cytoskeleton. *Cell* **164**, 433–446 (2016).
10. Romani, P. *et al.* Extracellular matrix mechanical cues regulate lipid metabolism through Lipin-1 and SREBP. *Nat Cell Biol* **21**, 338–347 (2019).

11. Bertolio, R. *et al.* Sterol regulatory element binding protein 1 couples mechanical cues and lipid metabolism. *Nat Commun* **10**, 1–11 (2019).
12. Helle, S. C. J. *et al.* Mechanical force induces mitochondrial fission. *Elife* **6**, 1–26 (2017).
13. Tharp, K. M. *et al.* Adhesion-mediated mechanosignaling forces mitohormesis. *Cell Metab* **33**, 1322-1341.e13 (2021).
14. Koo, J. H. & Guan, K. L. Interplay between YAP/TAZ and Metabolism. *Cell Metab* **28**, 196–206 (2018).
15. Via, G. & Signaling, M. Stiffer Matrix Accelerates Migration of Hepatocellular Carcinoma Cells through Enhanced Aerobic. *Cancers (Basel)* **12**, 490–505 (2020).
16. Wu, Y., Zanotelli, M. R., Zhang, J. & Reinhart-King, C. A. Matrix-driven changes in metabolism support cytoskeletal activity to promote cell migration. *Biophys J* **120**, 1705–1717 (2021).
17. Hardie, D. G. AMP-activated protein kinase-an energy sensor that regulates all aspects of cell function. *Genes and Development* vol. 25 1895–1908 Preprint at https://doi.org/10.1101/gad.17420111 (2011).
18. Xie, J., Bao, M., Hu, X., Koopman, W. J. H. & Huck, W. T. S. Energy expenditure during cell spreading influences the cellular response to matrix stiffness. *Biomaterials* **267**, 120494 (2021).
19. Tan, M. J. *et al.* Antidiabetic Activities of Triterpenoids Isolated from Bitter Melon Associated with Activation of the AMPK Pathway. *Chem Biol* **15**, 263–273 (2008).
20. Ceddia, R. B. *et al.* Globular adiponectin increases GLUT4 translocation and glucose uptake but reduces glycogen synthesis in rat skeletal muscle cells. *Diabetologia* **48**, 132–139 (2005).
21. Marsin, A. S. *et al.* Phosphorylation and activation of heart PFK-2 by AMPK has a role in the stimulation of glycolysis during ischaemia. *Current Biology* **10**, 1247–1255 (2000).
22. Marsin, A. S., Bouzin, C., Bertrand, L. & Hue, L. The stimulation of glycolysis by hypoxia in activated monocytes is mediated by AMP-activated protein kinase and inducible 6-phosphofructo-2-kinase. *Journal of Biological Chemistry* **277**, 30778–30783 (2002).
23. O'Neill, H. M., Holloway, G. P. & Steinberg, G. R. AMPK regulation of fatty acid metabolism and mitochondrial biogenesis: Implications for obesity. *Mol Cell Endocrinol* **366**, 135–151 (2013).
24. Horman, S. *et al.* Activation of AMP-activated protein kinase leads to the phosphorylation of elongation factor 2 and an inhibition of protein synthesis. *Current Biology* **12**, 1419–1423 (2002).
25. Kim, J., Kundu, M., Viollet, B. & Guan, K. L. AMPK and mTOR regulate autophagy through direct phosphorylation of Ulk1. *Nat Cell Biol* **13**, 132–141 (2011).
26. Eble, J. A. & Niland, S. The extracellular matrix in tumor progression and metastasis. *Clin Exp Metastasis* **36**, 171–198 (2019).
27. Spill, F., Reynolds, D. S., Kamm, R. D. & Zaman, M. H. Impact of the physical microenvironment on tumor progression and metastasis. *Curr Opin Biotechnol* **40**, 41–48 (2016).
28. Hanahan, D. & Weinberg, R. A. Hallmarks of Cancer: The Next Generation. *Cell* **144**, 646–674 (2011).
29. Afifi, N. & Barrero, C. A. Understanding Breast Cancer Aggressiveness and Its Implications in Diagnosis and Treatment. *Journal of Clinical Medicine* vol. 12 Preprint at https://doi.org/10.3390/jcm12041375 (2023).
30. Conti, M. A. & Adelstein, R. S. Nonmuscle myosin II moves in new directions. *J Cell Sci* **121**, 11–18 (2008).
31. Vicente-Manzanares, M., Ma, X., Adelstein, R. S. & Horwitz, A. R. Non-muscle myosin II takes centre stage in cell adhesion and migration. *Nat Rev Mol Cell Biol* **10**, 778–790 (2009).
32. Sit, S. T. & Manser, E. Rho GTPases and their role in organizing the actin cytoskeleton. *Journal of Cell Science* vol. 124 679–683 Preprint at https://doi.org/10.1242/jcs.064964 (2011).
33. Katoh, K., Kano, Y. & Noda, Y. Rho-associated kinase-dependent contraction of stress fibres and the organization of focal adhesions. *Journal of the Royal Society Interface* vol. 8 305–311 Preprint at https://doi.org/10.1098/rsif.2010.0419 (2011).
34. Matthews, B. D. *et al.* Ultra-rapid activation of TRPV4 ion channels by mechanical forces applied to cell surface β1 integrins. *Integrative Biology* **2**, 435–442 (2010).
35. Shenoy, V. B., Wang, H. & Wang, X. A chemo-mechanical free-energy-based approach to model durotaxis and extracellular stiffness-dependent contraction and polarization of cells. *Interface Focus* **6**, (2016).
36. Mitrossilis, D. *et al.* Single-cell response to stiffness exhibits muscle-like behavior. *Proceedings of the National Academy of Sciences* **106**, 18243–18248 (2009).
37. Kovács, M., Thirumurugan, K., Knight, P. J. & Sellers, J. R. Load-dependent mechanism of nonmuscle myosin 2. *Proceedings of the National Academy of Sciences* **104**, 9994–9999 (2007).
38. Schiffhauer, E. S. *et al.* Mechanoaccumulative Elements of the Mammalian Actin Cytoskeleton. *Current Biology* **26**, 1473–1479 (2016).
39. Schiffhauer, E. S. *et al.* Myosin IIB assembly state determines its mechanosensitive dynamics. *Journal of Cell Biology* **218**, 895–908 (2019).
40. Guo, M. *et al.* Cell volume change through water efflux impacts cell stiffness and stem cell fate. *Proceedings of the National Academy of Sciences* **114**, E8618–E8627 (2017).
41. Zanotelli, M. R. *et al.* Regulation of ATP utilization during metastatic cell migration by collagen architecture. *Mol Biol Cell* **29**, 1–9 (2018).
42. Cao, X. *et al.* Multiscale model predicts increasing focal adhesion size with decreasing stiffness in fibrous matrices. *Proc Natl Acad Sci U S A* **114**, E4549–E4555 (2017).
43. Ban, E. *et al.* Mechanisms of Plastic Deformation in Collagen Networks Induced by Cellular Forces. *Biophys J* **114**, 450–461 (2018).
44. Wang, H., S, A. A., Chen, C. S., Wells, R. G. & Shenoy, V. B. Long Range Force Transmission in Fibrous Matrices Enabled by Tension-Driven Alignment of Fibers. doi:10.1101/048579.
45. Lachowski, D. *et al.* Substrate Stiffness-Driven Membrane Tension Modulates Vesicular Trafficking via Caveolin-1. *ACS Nano* **16**, 4322–4337 (2022).

46. Wang, W., Miller, J. P., Pannullo, S. C., Reinhart-King, C. A. & Bordeleau, F. Quantitative assessment of cell contractility using polarized light microscopy. *J Biophotonics* **11**, e201800008 (2018).
47. Hassan, S., Kim, J. & suo, Z. Polyacrylamide hydrogels. IV. Near-perfect elasticity and rate-dependent toughness. *J Mech Phys Solids* **158**, 104675 (2022).
48. Zimmerman, J. J., von Saint André-von Arnim, A. & McLaughlin, J. Chapter 74 - Cellular Respiration. in *Pediatric Critical Care (Fourth Edition)* (eds. Fuhrman, B. P. & Zimmerman, J. J.) 1058–1072 (Mosby, Saint Louis, 2011). doi:https://doi.org/10.1016/B978-0-323-07307-3.10074-6.
49. Lou, F., Curtin, N. A. & Woledge, R. C. The Energetic Cost of Activation of White Muscle Fibres from the Dogfish Scyliorhinus Canicula. *Journal of Experimental Biology* **200**, 495–501 (1997).
50. Crow, M. T. & Kushmerick, M. J. Correlated reduction of velocity of shortening and the rate of energy utilization in mouse fast-twitch muscle during a continuous tetanus. *Journal of General Physiology* **82**, 703–720 (1983).
51. Baker, A. J. *et al.* Energy use by contractile and noncontractile processes in skeletal muscle estimated by 31P-NMR. *American Journal of Physiology-Cell Physiology* **266**, C825–C831 (1994).
52. Derricks, K. E., Trinkaus-Randall, V. & Nugent, M. A. Extracellular matrix stiffness modulates VEGF calcium signaling in endothelial cells: individual cell and population analysis. *Integrative Biology* **7**, 1011–1025 (2015).
53. Wicher, S. A. *et al.* Aging increases senescence, calcium signaling, and extracellular matrix deposition in human airway smooth muscle. *PLoS One* **16**, (2021).
54. Kim, T. J. *et al.* Substrate rigidity regulates Ca2+ oscillation via RhoA pathway in stem cells. *J Cell Physiol* **218**, 285–293 (2009).
55. Luo, M. *et al.* Compression enhances invasive phenotype and matrix degradation of breast Cancer cells via Piezo1 activation. *BMC Mol Cell Biol* **23**, (2022).
56. Kim, T. J., Sun, J., Lu, S., Qi, Y. X. & Wang, Y. Prolonged mechanical stretch initiates intracellular calcium oscillations in human mesenchymal stem cells. *PLoS One* **9**, (2014).
57. Richter, R. P. *et al.* Glycocalyx heparan sulfate cleavage promotes endothelial cell angiopoietin-2 expression by impairing shear stress-related AMPK/FoxO1 signaling. (2022) doi:10.1172/jci.
58. Mcgee, S. L. & Hargreaves, M. *AMPK and Transcriptional Regulation*. *Frontiers in Bioscience* vol. 13 (2008).
59. Lo, C.-M., Wang, H.-B., Dembo, M. & Wang, Y. Cell Movement Is Guided by the Rigidity of the Substrate. *Biophys J* **79**, 144–152 (2000).
60. Pakshir, P. *et al.* Dynamic fibroblast contractions attract remote macrophages in fibrillar collagen matrix. *Nat Commun* **10**, (2019).
61. Khetan, S. *et al.* Degradation-mediated cellular traction directs stem cell fate in covalently crosslinked three-dimensional hydrogels. *Nat Mater* **12**, (2013).
62. Cóndor, M. *et al.* Breast Cancer Cells Adapt Contractile Forces to Overcome Steric Hindrance. *Biophys J* **116**, 1305–1312 (2019).
63. Graham, D. M. *et al.* Enucleated cells reveal differential roles of the nucleus in cell migration, polarity, and mechanotransduction. *Journal of Cell Biology* **217**, 895–914 (2018).
64. Han, Y. L. *et al.* Cell contraction induces long-ranged stress stiffening in the extracellular matrix. *Proc Natl Acad Sci U S A* **115**, 4075–4080 (2018).
65. Yeung, T. *et al.* Effects of substrate stiffness on cell morphology, cytoskeletal structure, and adhesion. *Cell Motil Cytoskeleton* **60**, 24–34 (2005).
66. Alisafaei, F., Jokhun, D. S., Shivashankar, G. V. & Shenoy, V. B. Regulation of nuclear architecture, mechanics, and nucleocytoplasmic shuttling of epigenetic factors by cell geometric constraints. *Proc Natl Acad Sci U S A* **116**, 13200–13209 (2019).
67. Kozlov, M. M. & Chernomordik, L. V. Membrane tension and membrane fusion. *Current Opinion in Structural Biology* vol. 33 61–67 Preprint at https://doi.org/10.1016/j.sbi.2015.07.010 (2015).
68. Lombardi, M. L. *et al.* The Interaction between Nesprins and Sun Proteins at the Nuclear Envelope Is Critical for Force Transmission between the Nucleus and Cytoskeleton*. *Journal of Biological Chemistry* **286**, 26743–26753 (2011).
69. Ketema, M. & Sonnenberg, A. Nesprin-3: a versatile connector between the nucleus and the cytoskeleton. *Biochem Soc Trans* **39**, 1719–1724 (2011).
70. Chancellor, T. J., Lee, J., Thodeti, C. K. & Lele, T. Actomyosin Tension Exerted on the Nucleus through Nesprin-1 Connections Influences Endothelial Cell Adhesion, Migration, and Cyclic Strain-Induced Reorientation. *Biophys J* **99**, 115–123 (2010).